Tectonophysics 884 (2024) 230397

Contents lists available at ScienceDirect

Tectonophysics

journal homepage: www.elsevier.com/locate/tecto

A revolution in understanding SE Asia geodynamics since 20.5–18 Ma

Jean-Claude Sibuet [a,b,c], Siqing Liu [d,e,a,*], Minghui Zhao [a,f,**], Wen-Nan Wu [g], Yih-Min Wu [h], Jinhui Cheng [a,f], Jonny Wu [i,j]

[a] Key Laboratory of Ocean and Marginal Sea Geology, South China Sea Institute of Oceanology, Chinese Academy of Sciences, Guangzhou 511458, China
[b] 44 rue du Cloître, 29280 Plouzané, France
[c] Ifremer Centre de Brest, B. P. 70, 29280 Plouzané Cedex, France
[d] Guangzhou Marine Geological Survey, Guangzhou 511458, China
[e] Key Laboratory of Marine Mineral Resources, Ministry of Natural Resources, Guangzhou 511458, China
[f] University of Chinese Academy of Sciences, Beijing 100049, China
[g] Department of Earth Sciences, National Central University, Taoyuan 32001, Taiwan
[h] Department of Geosciences, National Taiwan University, No. 1, Section 4, Roosevelt Road, Taipei 10617, Taiwan
[i] Department of Earth and Atmospheric Sciences, University of Houston, 3057 Cullen Boulevard, Houston, TX 77204, USA
[j] Department of Geosciences, University of Arizona, Tucson, AZ, USA

ARTICLE INFO

Keywords:
South China Sea marginal sea
Okinawa trough opening
Manila transcurrent fault
Age Luzon arc and forearc
South China Sea seafloor spreading age
Plate kinematic reconstructions

ABSTRACT

We present an updated evaluation of SE Asian geodynamics that includes the interactions of the South China Sea (SCS) marginal basin with surrounding plates since the end of SCS spreading 20.5–18 Ma. Newly available Ar^{39}/Ar^{40} ages of SCS oceanic crust drilled at IODP U1431 near the SCS East basin extinct spreading center are older than 18 Ma. Conversely, the oldest ages of the Luzon arc and forearc at Taiwan's Lanyu island, Coastal range and Lichi mélange are 17–18 Ma, suggesting that onset of the Manila subduction zone may have begun a few m.y. earlier. Before ~20.5 Ma, the northern part of the Manila transcurrent fault (MTF), considered as the western boundary of the Ryukyu subduction zone, was a left-lateral lithospheric-scale shear zone. From ~20.5–18 Ma to ~7 Ma, this portion of MTF was connected to the Manila trench. Since ~7 Ma, the MTF extended into the Taiwan Longitudinal valley and continued southwards to north Luzon island as near-vertical, left-lateral shear zone. Today, south of ~24°N, the MTF protrudes down to 30 km depths and terminates above the deeper Manila slab. Since ~7 Ma, the whole MTF shifted 400 km westward with respect to Eurasia and rotated ~23° clockwise to become oriented ~NS north of 16°N latitude. We identify a tear fault in the Eurasian (EU) plate north of the Ryukyu trench that is located south of the Myako and Yonaguni islands. Since ~10 Ma, the tear continuously progressed westward within EU crust, with the Philippine Sea plate progressively subducting northwestward between the two lips of the tear fault. A RFF (ridge-fault-fault) triple junction was active in the EU crust before 20.5 Ma, from 10 to 7 Ma, and since 2 Ma. This triple junction was always located on the MTF with one branch of the MTF on each side of the triple junction, and the third branch being the spreading center.

1. Introduction

In the literature, marginal seas are extensional basins generated in a convergent plate setting (Mohn et al., 2022) and include backarc basins (*e.g.* Karig, 1971). They are the most complex tensional systems formed on the earth's surface. The South China Sea (SCS) is such an extensional basin, which formed and evolved since the earliest Tertiary behind a ~NS-verging subduction zone, coupled with the simultaneous proto-SCS subduction (Sibuet et al., 2021; Mohn et al., 2022). Variations in the subduction zone characteristics, such as the direction of convergence, the dip, or the subduction velocity (*e.g.* Sibuet et al., 2016; van de Lagemaat and van Hinsbergen, 2024), result in changes in the directions in which the seafloor spreads and the occurrence of ridge jumps (Guan et al., 2021).

To better understand this environment, new research fields were developed during the last ten years: amongst them, new revolutionary

* Corresponding author at: Guangzhou Marine Geological Survey, Guangzhou 511458, China.
** Corresponding author at: Key Laboratory of Ocean and Marginal Sea Geology, South China Sea Institute of Oceanology, Chinese Academy of Sciences, Guangzhou 511458, China.
E-mail addresses: lsq13140307@126.com (S. Liu), mhzhao@scsio.ac.cn (M. Zhao).

https://doi.org/10.1016/j.tecto.2024.230397
Received 27 April 2023; Received in revised form 17 June 2024; Accepted 18 June 2024
Available online 22 June 2024

plate kinematic reconstructions (*e.g.* Wu et al., 2016; Wu and Suppe, 2018; Advokaat et al., 2018; van de Lagemaat and van Hinsbergen, 2024; Zhao et al., 2019) with testable paleolatitude evolution, mantle structure and magmatic activity are made possible by the East Asian plate tectonics, which has resulted in slabs unfolding and restoring on the Earth's surface since 52 Ma. In parallel, significant advancements were made in determining the age of igneous rocks and the nature of the crust that was penetrated during the ascent of magma. The isotopic composition of rock samples and melt intrusions give now unprecedented constraints on the mantle source heterogeneity resulting from the underlying presence of subducted sediments and oceanic or continental crust (*e.g.* Wu and Wu, 2019; Qian et al., 2022). The combined use of these methods will allow us to propose new concepts for the formation and evolution of SCS marginal sea or to validate already published concepts.

At crustal and upper mantle scales, tomographic data obtained from seismic refraction profiles with closely spaced ocean bottom seismometers (OBSs) collected with coincident deep multi-channel seismic (MCS) profiles, and industrial or IODP boreholes information bring solid constraints concerning the age and nature of the high-velocity layer (HVL) located at the base of the thinned continental crust, the nature of upper mantle and the geographic extension and internal structure of the continent-ocean transition zone (COT) (*e.g.* Deng et al., 2020; Ding et al., 2020; Liu et al., 2022; Mohn et al., 2022; Mi et al., 2023).

In the SCS, the COT is located between the thinned continental crust and the oceanic domain. The continent-ocean boundary (COB) is a different concept in comparison with the COT and generally corresponds to the oceanward boundary of the COT. In the southern Ryukyu subduction zone, the Eurasian (EU) COT cannot be defined on tomographic images of unfolded slabs because *Vp* or *dVp* values display a gradient, which only allows to approximately define a COB set up in the middle part of this gradient (Liu et al., 2018).

Only publications using tomographic images, coincident seismic refraction and MCS profiles, modern geochemistry methods or borehole data can be considered as reliable for establishing SE Asia geodynamic constraints. We will demonstrate that a) the oldest age of the Luzon arc and forearc is 17–18 Ma; b) the age of the end of SCS seafloor spreading is older than ~18 Ma rather than 15.5–16 Ma as commonly proposed; c) the existence of a transcurrent shear zone called the Manila transcurrent fault (MTF) constrains the understanding of the EU)/Philippine Sea plate (PSP) motion since ~7 Ma; d) how the geometry and nature of the northeastern SCS margin is accommodated in the Taiwan region during the Luzon arc and forearc collision with the EU continent; e) we will confirm that the Okinawa trough (OT) opening occurred simultaneously with the eastward propagation of a tear fault (Lallemand et al., 2013); and, f) using these constraints, we will present and discuss a series of five plate kinematic reconstructions, spanning since ~20.5 to ~18 Ma.

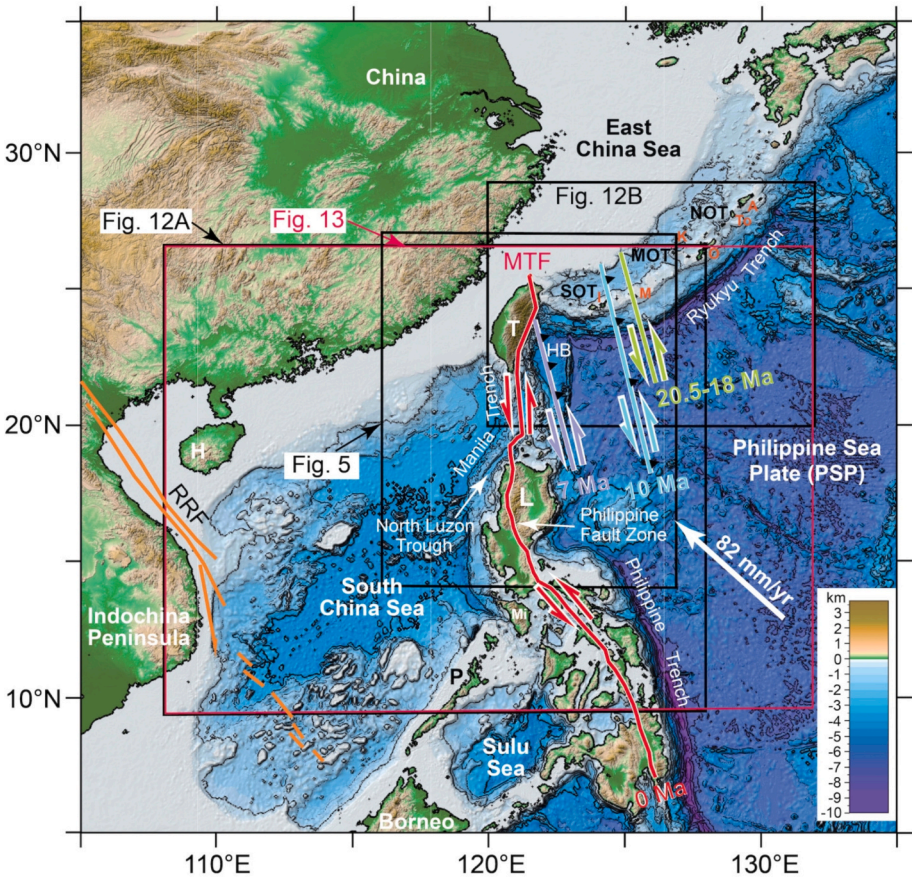

Fig. 1. Bathymetric map of SE Asia with HB-PSP/EU shear plate boundaries at ~20.5- ~18 Ma, ~10, ~7 Ma and Present. For clarity, only the Present HB-PSP/EU shear plate boundary (continuous red line) extends to the south.
The rectangles are locations of the main figures shown in the text. A, Amami island; EU, Eurasian plate; H, Hainan; HB, Huatung basin; I, Ishigaki island; K, Kume island; L, Luzon island; M, Miyako island; Mi, Mindoro island; MOT, middle Okinawa trough; NOT, northern Okinawa trough; O, Okinawa island; P, Palawan; PSP, Philippine Sea plate; RRF, Red River fault system; SOT, southern Okinawa trough; T, Taiwan island; To, Tokuno island. (For interpretation of the references to colour in this figure legend, the reader is referred to the web version of this article.)

2. Ages of SCS seafloor spreading and of the onset of Luzon arc and forearc

2.1. Age of the end SCS seafloor spreading

The SCS is bounded to the north by the South China margin, to the south by the Borneo and Palawan margins, to the east by the Manila trench and to the west by the Red River fault system, which continues to the south along the Vietnamese margin and the Sunda shelf (Fig. 1). Concerning the South China Sea oceanic opening in the east and southeast basins, two competing hypotheses exist (Fig. 2) (Briais et al., 1993; Barckhausen et al., 2014). Briais et al. (1993) presented the interpretation of a relatively dense set of marine magnetic profiles with a synchronous cessation of seafloor spreading in the east and southwest basins at ~15.5 Ma, just after chron C5c (16 Ma). Seafloor spreading was asymmetric with two ridge jumps located north of the extinct spreading center, at chrons C10 (30 Ma) and C7 (25 Ma) (Fig. 2A). Barckhausen et al. (2014) acquired a series of well-located magnetic profiles and suggest that seafloor spreading stopped at the same time in the east and southwest basins, at chron C6a1 dated 20.5 Ma. They also identified a ridge jump at chron C7 (Fig. 2B). The onset of seafloor spreading is relatively agreed between models (chron 11 at 32 Ma and chron 12 at 31 Ma, respectively), but the end of SCS seafloor spreading varies between 15.5 Ma (Briais et al., 1993) and 20.5 Ma (Barckhausen et al., 2014). This presents a significant difference in implied mean oceanic spreading rates between the two models, with a mean oceanic spreading rate ~ 50% larger for Barckhausen et al. (2014) compared to Briais et al. (1993).

Before Barckhausen et al. (2014), surface and deep tow magnetic survey results appeared to confirm the Briais et al. (1993) interpretation; for example, Li et al. (2014) and more recently Sun et al. (2019a) identified the end of SCS seafloor spreading at chron C5br (~15.5 Ma). Drilling close to the extinct spreading center at sites U1431 in the East basin, U1433 and U1434 in the southwest basin (Fig. 2) shows that the age of sediments at the contact with the underlying massive basaltic series are 13 Ma at U1431 and 15 Ma at U1433 (Li et al., 2015a), in accordance with Briais et al. (1993). Recently, Guan et al. (2021) used an unpublished high resolution dense magnetic dataset (Fig. S1A) to identify and date the magnetic lineations by considering that the onset and the end of SCS seafloor spreading occurred at 30 Ma and 15.6 Ma (chron 11n.1r to 5Br). The SCS East basin magnetic isochron pattern (Fig. S1B) displays ~NS fracture zones and five ridge jumps, suggesting that this geometry reflects the complex evolution of a marginal sea. The same magnetic pattern (Fig. S1C), re-interpreted by Wu et al. (2023) (Fig. S1D) in the northern part of the SCS, shows not only different locations for ridge jumps and fracture zones but different magnetic lineation dating. As this magnetic dataset is not publicly available, the location and age of the SCS seafloor spreading cannot be re-evaluated in this paper.

Site U1431 was drilled in the East basin, ~20 km north of the extinct spreading ridge (Fig. 2). Between the lower volcanoclastic series Unit VII and the upper massive lava flow series (Unit IX) lies the hemipelagic

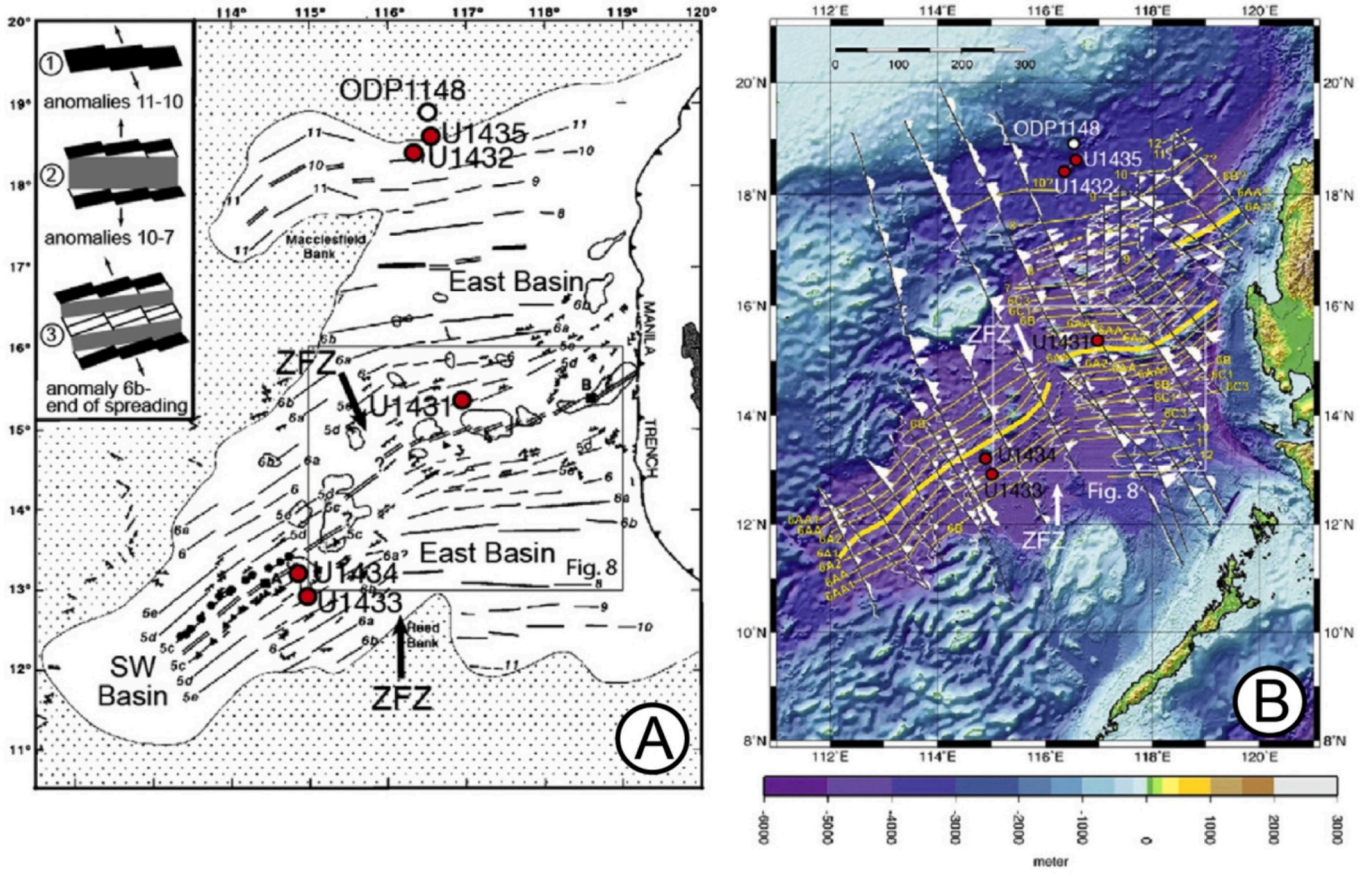

Fig. 2. Magnetic lineations in the South China Sea (SCS).
A) From Briais et al. (1993) with inset presenting their evolution of seafloor spreading geometry in the East basin. B) SCS bathymetric map with magnetic profiles shown as wiggles along ship tracks and magnetic anomaly interpretation (thin yellow lines) from Barckhausen et al. (2014). Thick yellow lines are abandoned spreading ridges and numbers indicate magnetic chrons. White dot, ODP Site 1148; red dots, Leg 349 IODP Sites; ZFZ, Zhongnan fracture zone. Discussion and detailed informations in Sibuet et al. (2016). (For interpretation of the references to colour in this figure legend, the reader is referred to the web version of this article.)

claystone Unit VIII (Fig. 3A). Based on foraminifers and nannofossils, Unit VIII is ~13 Ma old (Li et al., 2015b). Inside the underlying massive lava flows series, the claystone Unit X does not contain *in situ* calcareous microfossils, but radiolarians, generally highly dissolved, corresponding to radiolarian zone RN4 of early Miocene age (~16.7–17.5 Ma) (Li et al., 2015a). If these ages are correct, basalts of Unit XI cored below Unit X must be older than ~16.7–17.5 Ma, which tends to contradict the younger ages of Briais et al. (1993). To clarify this point, we tried to find Ar^{39}/Ar^{40} basalt analyses performed in the massive lava flows series Units IX and XI. We have found two sources (Fig. 3A). Koppers (2014) gives ages of ~15 Ma in Unit IX and ~ 17 Ma in Unit XI. Preliminary unpublished ages slightly older than 18 Ma were recently found in Units IX and XI (Huang X.L., personal communication, November 2023). It suggests that the 18 Ma age at which seafloor spreading ceased in Unit XI, and consequently in the East basin, are incompatible with the Briais et al. (1993) hypothesis. To clarify this point, additional Ar^{39}/Ar^{40} basalt

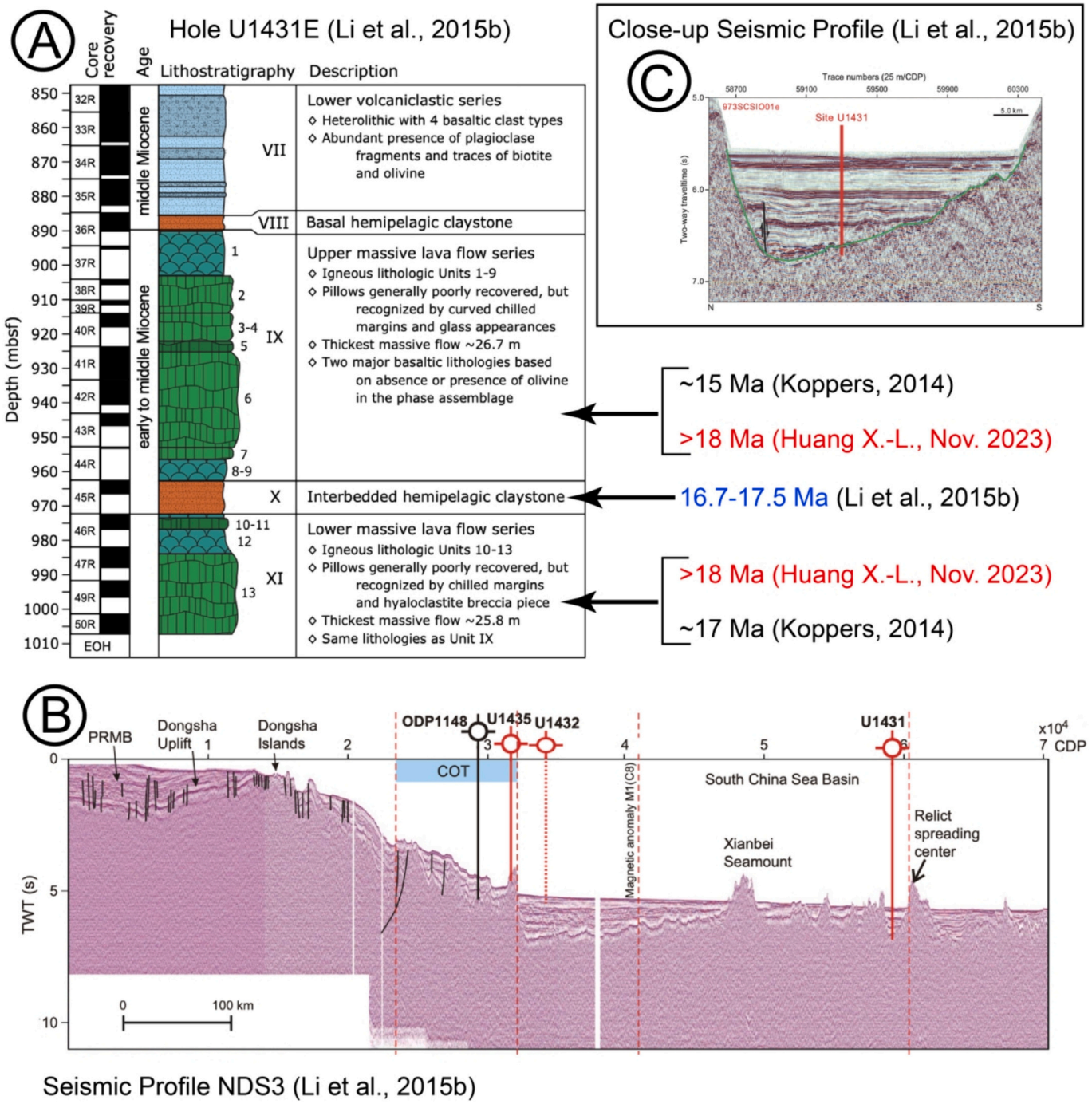

Fig. 3. Age of end of seafloor spreading in the South China Sea.
A) Hole U1431E lithostratigraphy of massive lava flow series (Units IX and XI) and overlying sediments (Unit VIII) (Li et al., 2015b). Ar^{39}/Ar^{40} ages in black (Koppers, 2014) and in red (Huang X.L., personal communication, 2013). In blue, ages of the hemipelagic layer of claystone (Unit X) based on radiolarians (Li et al., 2015b). B) The oceanic domain located south of the continental oceanic transition (COT) on seismic profile NDS3 (Li et al., 2015b) is everywhere affected by post-spreading magmatism, except in the deep depression where Site U1431 was drilled. C) Close-up of seismic profile NDS3 with location of Site U1431. A 150 to 200 m-thick high-amplitude sedimentary layer located above the axial part of the depression was not drilled (green line). (For interpretation of the references to colour in this figure legend, the reader is referred to the web version of this article.)

analyses in the two massive lava flows series are underway (Huang X.L., personal communication, November 2023).

The NS NDS3 oriented seismic profile across the East basin (Li et al., 2015b) shows that post-rift magmatism everywhere distorts the basement geometry south of the Xianbei seamount and has a significant impact on the oceanic crust (Fig. 3B). The only exception is located close to the extinct spreading center where IODP Hole U1431 was drilled. It appears that this is the only site near the extinct spreading center where typical oceanic crust can be drilled in a small depression, or possibly in an ~EW elongated sub-basin approximately orthogonal to the NDS3 profile, as the overlying sediments are not distorted by post-rift magmatism. Site U1431 is slightly offset from the deepest part of the depression (close-up in Fig. 3C). At Site U1431, 13 Ma old pelagic sediments were drilled above of the oceanic basement in Unit VIII (Li et al., 2015b), while 150 to 200 m of pelagic sediments older than 13 Ma are present in the deepest part of the depression (Fig. 3C). Using sedimentation rates calculated in the lower pelagic sedimentary series, the oldest basement age in the deepest part of the depression would be between 15 and 18 Ma; this age range is too wide to constrain the time that SCS spreading ended. Therefore, to overcome this problem, detailed Ar^{39}/Ar^{40} measurements are still necessary within Units IX and XI, even if arguments concerning the oldest age of the Luzon arc will bring additional arguments in favor of a > 18 Ma old oceanic crust at site U1431.

2.2. Oldest age of Luzon arc and forearc formation

On each side of the Longitudinal valley of Taiwan, the East Taiwan ophiolite (ETO) (Fig. 4B and C) corresponds to the northern prolongation of the Luzon forearc (Fig. 4B) that deformed and uplifted during the Luzon arc collision with the EU continent (Chen et al., 2017). It comprised the Lichi mélange exposed along the western border of the Coastal range (accreted Luzon arc) and the Yuli belt, a Miocene subduction complex juxtaposed east of the exhumed EU continental margin basement. At Site JW02 (Fig. 4C), a 17.79 +/− 0.40 Ma gabbro was found (Lo et al., 2020) (Zircon -Pb Laser Ablation Analysis). Independently, a plagiogranite and a gabbro block collected in the Lichi mélange near Site JW02 (Fig. 4C) are 17.21 ± 0.32 Ma and 17.34 ± 0.35 Ma old respectively (Huang et al., 2018) (SIMS on zircon grains). In a more recent study in the same area of the Lichi mélange, Yu et al. (2022) found that ~17.3 Ma old adakitic dikes (εNd of 7.4–7.9 and $^{206}Pb/^{204}Pb$ of 18.27–18.42) were simultaneously crystallized with normal and enriched 17.8–14.1 Ma old mid-oceanic ridge N- and *E*-MORB basalts (εNd of 8.8–13.3 and $^{206}Pb/^{204}Pb$ of 17.71–18.22). Yu et al. (2022) conclude that the middle Miocene ophiolitic blocks of the East Taiwan ophiolite are on-land Luzon forearc basement blocks. Therefore, the oldest age of formation of the Luzon forearc samples in the Lichi mélange is 17–18 Ma. However, note that both in the Lichi mélange and in the Yuli belt (Fig. 4C), at Site JW01 and Site WL02 (Fig. 4C) respectively, Lo et al. (2020) also published $^{206}Pb/^{238}U$ ages of 14.67 +/− 0.19 Ma in a chert and 14.98 +/− 0.22 Ma in a meta-gabbro. The meaning is not clear, as Lo et al. (2020) interpret these results as linked to relicts of subducted SCS oceanic crust with intermingled siliceous rocks.

The age of the oldest Luzon arc volcanism obtained in Lanyu island (Fig. 4A) comes from a study of sedimentary fragments interbedded in volcanic rocks with calcareous nanoplanktons belonging to the NN3 zone (17–18 Ma, Chi and Suppe, 1985). Consequently, both the Luzon arc and forearc started to form approximately at the same time, 17–18

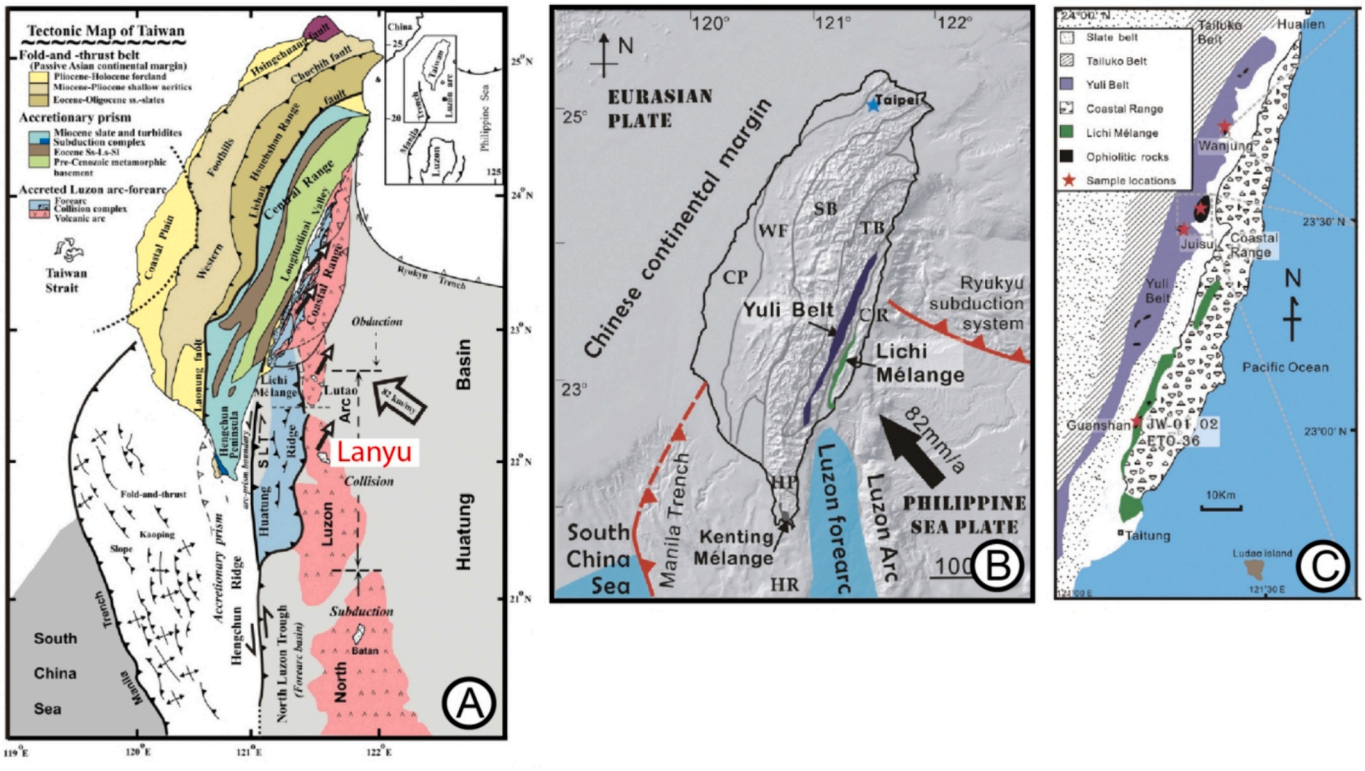

Fig. 4. Determination of the oldest ages of the Luzon arc and forearc.
A) On Huang et al. (2018) synthetic map, the oldest age of Luzon arc is 18–20 Ma on Lanyu island (Chi and Suppe, 1985). B) and C) On Lo et al. (2020) geological maps, the east Taiwan ophiolite (ETO) is composed of the Lichi mélange (in green) and the Yuli belt (in blue or purple). The oldest ages found on a gabbro at sampling Site JW02 in the Lichi mélange (red star in C) are ~17,79 +/− 0,40 Ma. The same ages are also found by Yu et al. (2022) and Huang et al. (2018) on samples collected in the vicinity of Site JW02. All datations suggest that the oldest age of the Luzon forearc and arc in the ETO is ~18 Ma. The Manila subduction zone must have reached a minimum depth of 80 km before the intra-oceanic Luzon arc could outcrop at the sea-bottom, suggesting the Manila subduction initiation might have started ~20.5 Ma ago. (For interpretation of the references to colour in this figure legend, the reader is referred to the web version of this article.)

Ma ago. As the Manila slab must have reached a minimum depth of 80 km before the 17–18 Ma intra-oceanic Luzon arc could outcrop at the sea-bottom, the Manila subduction zone initiation might have started a few m.y. before, perhaps at ~20.5 Ma, the end of SCS seafloor spreading for Barckhausen et al. (2014).

At Site U1431, the age of the oceanic crust is slightly older than ~18 Ma, which suggests that either the end of SCS seafloor spreading is ~18 Ma or maybe ~20.5 Ma as suggested by the Barckhausen et al. (2014) magnetic modeling. If the end of SCS seafloor spreading occurred at ~20.5 Ma, the Manila subduction zone initiation would have also occurred at the same time, ~20.5 Ma ago. On the contrary, if the end of SCS seafloor spreading occurred at ~18 Ma, the Manila subduction zone would have been simultaneously active with SCS seafloor spreading between ~20.5 and ~ 18 Ma (*i.e.* spreading ridge subduction). However, it seems difficult to open the SCS in a ~ NS direction simultaneously with the southward subduction of the Proto-SCS, while the PHP/EU motion occurs in the N-NW direction (Sibuet et al., 2021). A prominent present-day example is the subduction of the south Chile active spreading ridge (Sisson et al., 2003; Boutonnet et al., 2010), which occurs in the simple geodynamic context of a Ridge-Fracture-Fracture (RFF) triple junction. Due to this uncertainty, we suggest that the end of SCS seafloor spreading occurred between ~20.5 and ~ 18 Ma, without choosing a specific option.

3. The Manila transcurrent fault (MTF): A major plate boundary controlling the SE Asia geodynamic evolution

Today, the MTF is an active left-lateral shear fault, which extends

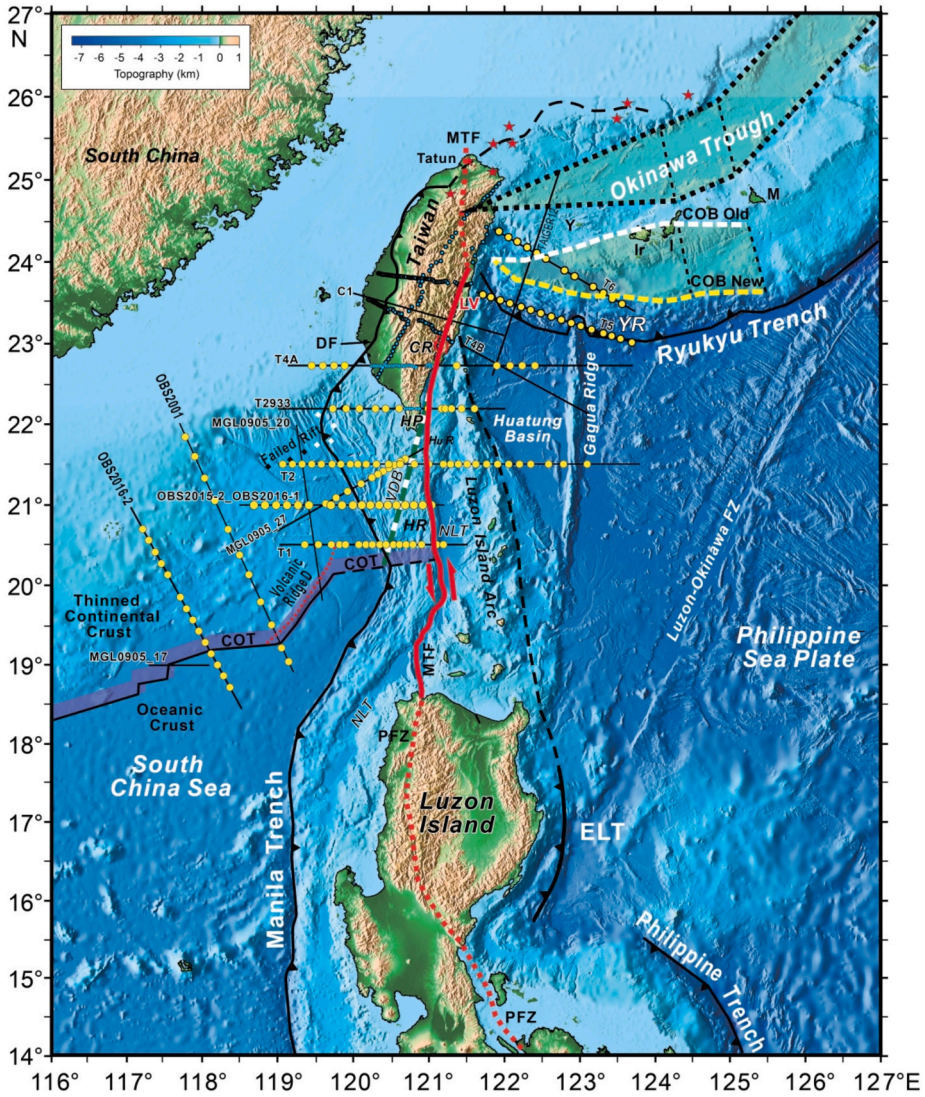

Fig. 5. Bathymetric map of study area (Barckhausen et al., 2014) with major tectonic features.
Wide-angle seismic refraction profiles (yellow dots) and associated MCS lines (thin continuous black lines) plus a few MCS lines discussed in the text. The NE-SW oriented failed rift (black and white diamonds) is from McIntosh et al. (2014). The continent-ocean transition zone (COT) refined in this study is the continuous black line with its width given by the adjacent purple line. The intra-continental velocity difference boundary (VDB, green and white dashed line) is the boundary between two types of thinned continental crusts with minor velocity differences (see text for further explanations). Black lines with triangles are the Manila trench extended by the Deformation front (DF) in the north, the Philippine trench and the East Luzon trough (ELT). The red continuous line is the left-lateral Manila transcurrent fault (MTF) extended to the south by the Philippine fault zone (PFZ, red dashed line) and to the north up to the Tatun volcano (red dashed line). The area between COB Old (white dashed line) and COB New (yellow dashed line) gives the whole amount of extension during the Okinawa trough (OT) opening (southern light green area) transferred in the OT basin (northern light green area). Red stars, volcanoes; CR, Central ridge; HP, Hengchun peninsula; HR, Hengchun ridge; HuR, Huatung ridge; LV, Longitudinal valley; NLT, north Luzon trough. (For interpretation of the references to colour in this figure legend, the reader is referred to the web version of this article.)

from the Philippine fault zone (PFZ) to the north of Taiwan (Sibuet et al., 2021) (Figs. 1 and 5). In detail, from south to north, the MTF follows a) the Philippine fault zone (PFZ); b) a segment between north Luzon island and the Hengchun peninsula; c) the continental slope of the portion of margin located east of Hengchun peninsula; d) the Longitudinal valley; e) a NS trend from the northern part of the Longitudinal valley to the Tatun volcano, continuing a few kilometers north of the Taiwan coast. The MTF is shown as a throughgoing fault in Fig. 5, which is suitable for the regional tectonic analysis here, but at smaller scales the MTF is likely expressed in the upper crust as a series of linked, left-lateral shear zone segments.

3.1. *The Philippine fault zone is the southern prolongation of the MTF*

The PFZ consists of a series of pseudo-parallel left-lateral shear faults active since the middle to late Miocene, oriented ~NS in north Luzon island and ~ N320° southward 16°N latitude (Barrier et al., 1991; Aurelio et al., 2014) (Figs. 1 and 5). North of 16°N, the PFZ (dashed red line in Fig. 5) and the MTF approximately follow the 121°E meridian. For Aurelio (2000), the PFZ first appeared ~10 Ma ago south of 16°N latitude and then in the north of Luzon island ~4 Ma ago. These ages are poorly constrained and suggest that the MTF was perhaps recently active (since ~7 Ma, the age of Luzon arc and forearc collision with EU?). Though imprecise, left-lateral slip rates are between 25 mm/yr (Barrier et al., 1991) and 35 mm/yr (Aurelio et al., 1997) along the PFZ. A correlation between the PFZ and the Longitudinal valley is suggested by comparable left-lateral slip rates of 30 mm/yr along the Longitudinal valley (Yu and Kuo, 2001). However, concurrent intraplate motions have been observed along the Gagua ridge in the PSP plate since ~10 Ma (Huang et al., 2001; Eakin et al., 2015; Sibuet et al., 2021) and in Taiwan (*e.g.* Lee et al., 1997; Conand et al., 2020) since ~7 Ma (Lin et al., 2003). These observations imply that the MTF-PFZ left-lateral shear fault is a moving feature with respect to EU, both in space and time.

Today, the Philippine mobile belt extends between the Manila subduction zone and the East Luzon trough-Philippine subduction zones (Fig. 5). Its northern prolongation includes the Luzon arc and forearc. The western boundary follows the Longitudinal valley and then the eastern limit of the Manila and Negros accretionary prisms (*e.g.* Aurelio et al., 2014). Its eastern boundary follows the eastern boundary of the Coastal range and Luzon island arc (dashed black line in Fig. 5). In north Luzon island, the basement rocks consist of ophiolites, continental blocks and intruded Cretaceous to Quaternary magmatic arcs (*e.g.* Polvé

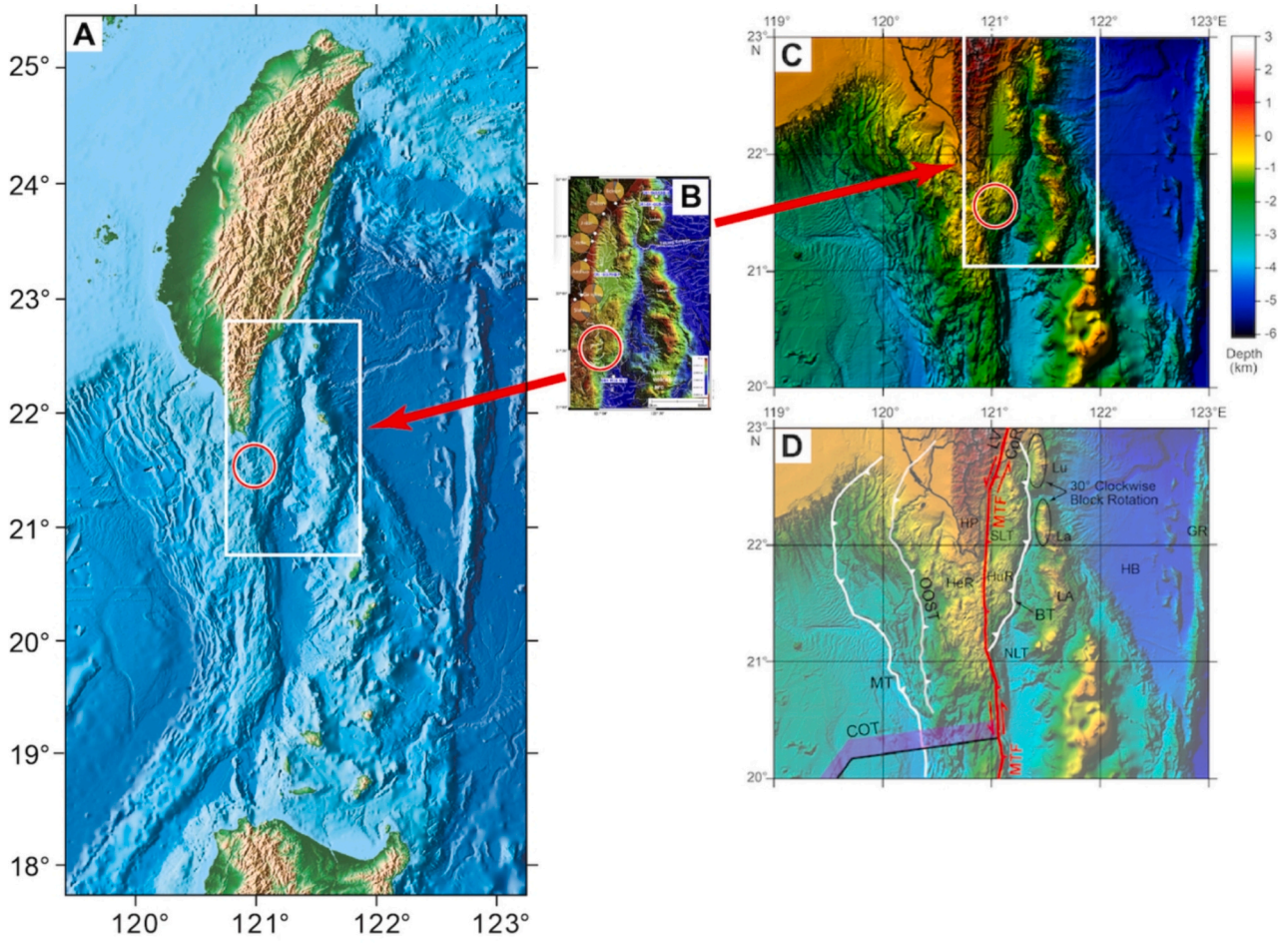

Fig. 6. Manila transcurrent fault (MTF) identification on swath bathymetric data between Taiwan and northern Luzon island.
A) Swath bathymetric data (Barckhausen et al., 2014) interpreted in Fig. 5 shows here where the MTF is located south of the Longitudinal valley, along the continental slope east of the Hengchun peninsula, and then, west of the Southern Longitudinal trough and the North Luzon trough (Fig. 4A). To the south, the MTF is connected to the Philippine fault zone (PFZ) located in the northern Luzon island (Sibuet et al., 2021). B) Swath bathymetric data processed by Nayak et al. (2021). Canyons are shown by thin white lines. C) Swath bathymetric data processed in Sibuet et al. (2021) and including recent data collected around Taiwan. Red circles in A, B and C exemplify the area where the MTF continuity is questionable, south of the Hengchun peninsula. In B, most of the minor canyon trends stop along an NS elongated depression with highs and lows, suggesting a continuity along the MTF trend. D) Location of the MTF (red continuous line) with respect to surrounding features. CoR, Coastal range; COT, Continent-ocean transition zone; GR, Gagua ridge; HB, Huatung basin; HeR, Hengchun ridge; HP, Hengchun peninsula; HuR, Huatung ridge; La, Lanyu Island; LA, Luzon arc; Lu, Lutao Island; LV, Longitudinal valley; MT, Manila trench; NLT, north Luzon trough; OOST; out-of-sequence thrust; SLT, southern Longitudinal trough. (For interpretation of the references to colour in this figure legend, the reader is referred to the web version of this article.)

et al., 2007). The Philippine mobile belt boundaries were changing location in space and through time since ~20.5 - ~18 Ma and earlier (Wu et al., 2016; Lallemand, 2016).

3.2. The MTF between the Philippine fault zone and the Longitudinal valley

The MTF (Fig. 5) can be followed on the swath bathymetric map of Fig. 6A, from the north Luzon coast, where Armada et al. (2013)

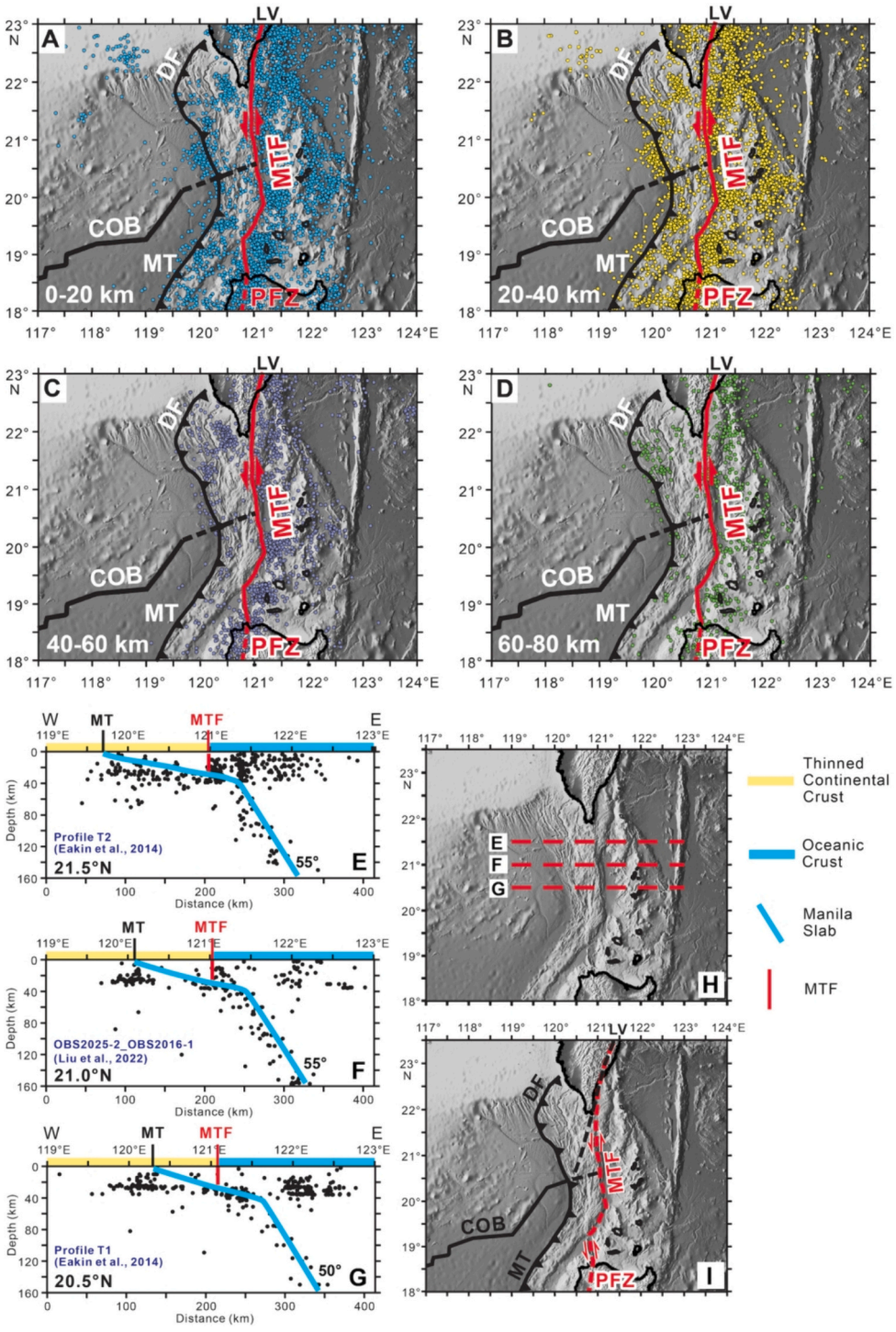

Fig. 7. The Manila transcurrent fault (MTF) is a major upper crustal feature active since ~7 Ma (modified from Liu et al., 2022).
A) to D) Earthquakes from the International Seismological Centre (ISC) database with a magnitude >4 for 20-km thick slices from 0 to 80 km. E) to G) Vertical cross-sections showing the same earthquakes within a bandwidth of 30 km along each side of the profiles. No vertical exaggeration. The thick colored lines on top of the cross-sections represent the Eurasia thinned continental crust and mantle in yellow and the oceanic crust and mantle in blue. The approximative dip of the Manila slab (thin light blue lines) is based on the same distribution of EQs. H) Location of profiles E, F and G (red dashed lines). I) Location of the present-day continent-ocean boundary (COB, continuous black line), which abuts the MTF. DF, Deformation front; LV, Longitudinal valley; MT, Manila trench; PFZ, Philippine fault zone. (For interpretation of the references to colour in this figure legend, the reader is referred to the web version of this article.)

established the MTF follows the eastern border of a NS oriented feature, to the area of the red circle. In the red circle of Fig. 6C, the MTF continuity seems to be broken by three short topographic segments oriented ~N050° (Sibuet et al., 2021). In fact, the prominence of these topographic features is exaggerated by the DEM illumination (*i.e.* lighting angle) coming from NW on Fig. 6C. On Fig. 6B (Nayak et al., 2021), the illumination angle is from the NE and the morphology of these features are more realistic. Canyons shown by very thin white lines seem to be all coming from the Hengchun ridge and not from the Huatung ridge located further east (Fig. 6C and D). They all seem to reach a NS feature, which looks like a NS oriented canyon with some obstacles along its downslope trend. Thus, both in Nayak et al. (2021) (Fig. 6B) and in Huang et al. (2018) (Fig. 4A), the MTF corresponds to a continuous feature extending further south (Fig. 5).

Seismic events of magnitude >4 are plotted in 20-km thick slices down to 80 km (Fig. 7). Slices 0–20 km and 20–40 km (Fig. 7A and B) show that most of the seismic events are located between the MTF and the Luzon arc, from south of the Longitudinal valley to 19.2°N, where the MTF changes trend to become NS. However, several crustal and upper mantle patches are present between the MTF and the Manila trench that are not linked to the MTF. Slices 40–60 km and 60–80 km (Fig. 7C and D) show that upper mantle seismic events are located between the MTF and the Luzon arc, and between south of the Longitudinal valley to the coast of northern Luzon island. Seismic patches located west of the MTF are disconnected from the MTF. On slices deeper than 80 km, there are only a few seismic events located east of the MTF (Liu et al., 2022). Sibuet et al. (2021) wrongly interpreted the MTF as a vertical lithospheric feature down at least to ~70 km. The MTF does not extend deeper than ~30 km, which is the isoline depth of the Manila slab at the vertical below the MTF (Fig. 10A and Ustaszewski et al., 2012). In fact, the seismicity shows the progressive eastward deepening of the Manila slab east of the MTF. Fig. 7A to G show the location of the MTF with respect to the geometry of the Manila slab.

Shot at mid-distance between refraction profiles T1 and T2 (Fig. 8), the wide-angle refraction profile OBS2015-2_OBS2016–1 with OBS spacing of 15 km and the coincident MCS profile imaging the Moho are of high quality (Liu et al., 2022). The thinned continental crust, with a ~ 3 km thick HVL at its base, is subducting below the accretionary wedge (Hengchun ridge). However, as the tomography of the three refraction profiles does not extend to depths >20 km, it is difficult to correctly establish the topography of the slab and its relationship with the MTF. A main input of the refraction data is the identification of an intra-continental velocity difference boundary (VDB) located at mid-distance between the Manila trench and the MTF (Fig. 8) with slightly different velocity-depth profiles in the thinned continental crust on each side of it (Liu et al., 2022). The "undefined body", a 5.0 to 5.5 km/s body of thinned continental crust located above another portion of thinned continental crust (Fig. 8C), is what makes up the thinned continental crust between the VDB and the MTF (Liu et al., 2022). There is a velocity discontinuity near the base of the undefined body (Fig. 8C), which we assume is caused by the Manila slab following the base of the undefined body.

Based on the interpretation of refraction line OBS2015-2_OBS2016–1 (Fig. 8C), the interpretation of refraction profiles T1 and T2 (Eakin et al., 2014) was updated (Liu et al., 2022), the locations of the MTF and VDB were identified as well as the slightly different velocity structure of the thinned continental crust on each side of the VDB. The "undefined body" was pinpointed on T1 (Fig. 8D) while only suggested on T2 (Fig. 8B) because Eakin et al. (2014) refraction tomography does not reach enough depth. Thus, in Fig. 8, the roof of the Manila slab follows the base of the undefined body and the VDB line is located where the Manila slab begins to include further east some thinned continental crust. In plan, the VDB line established on profile OBS2015-2_OBS2016–1 and inferred on profiles T1 and T2 merges the MTF at the latitude of the Hengchun Peninsula (Figs. 5 and 8A). Thus, the interpretation of the three refraction profiles suggests that the Manila slab cuts the accretionary wedge and then the thinned continental crust (below the undefined body) east of the VDB. East of the MTF, the Manila slab is the

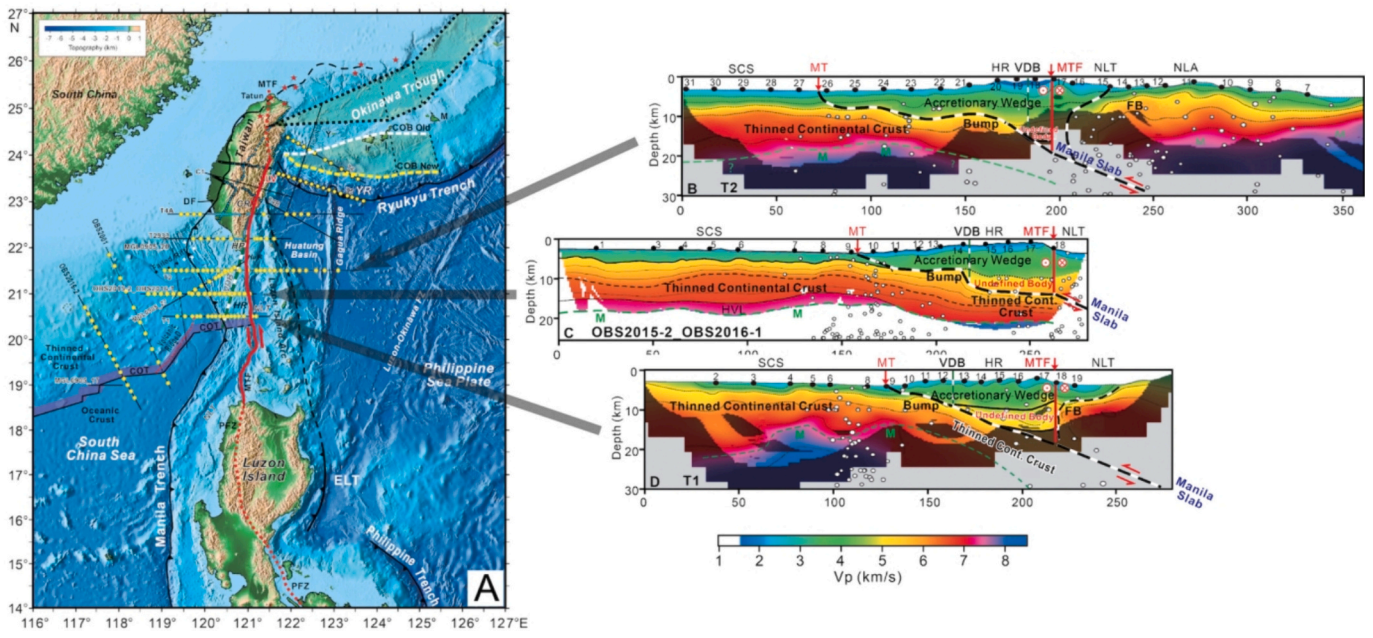

Fig. 8. The three refraction profiles (located in A) are aligned along the NS oriented MTF.
West of the MTF, the crust is thinned continental crust while east of the MTF, the subducted Manila crust is mainly oceanic. Wide-angle seismic profiles T2, OBS2015–2_OBS2016–1 and T1 displayed with a 2.5 vertical exaggeration. B) Profile T2 (Eakin et al., 2014) updated from Liu et al. (2022). C) Profile OBS2015–2_OBS2016–1 updated from Liu et al. (2022). D) Profile T1 (Eakin et al., 2014) updated from Liu et al. (2022). The Manila slab, dipping 55° along profiles T2 and OBS2015–2_OBS2016–1 and 50° along profile T1, is extracted from Fig. 7 but its location at depth is poorly defined. COB, continent-ocean boundary; COT, continent-ocean transition zone; FB, forearc block; HR, Hengchun ridge; M, Moho; MT, Manila trench; MTF, Manila transcurrent fault; NLA, north Luzon arc; NLT, north Luzon trough; SCS, South China Sea; VDB, intra-continental velocity difference boundary.

allochthonous oceanic PSP plate, which is moving in the northward direction. East of the MTF, the Manila slab is given for information only as it not constrained by refraction data (Fig. 8).

3.3. The MTF near the Longitudinal valley

Insights on the deformation pattern and stress regime are given by earthquake focal mechanisms. The moment tensor catalog AutoBATS, managed by the Data Management Center of the Institute of Earth Sciences, Academia Sinica (Institute of Earth Sciences, Taiwan, 1996), provides the moment tensor solutions for intermediate and large ($M > 3.5$) earthquakes occurring in the Taiwan region between March 1996 and December 2023. The moment tensor solutions are determined by waveform inversion based on a fully automated parameter-scanning algorithm (Jian et al., 2018), and provide a reliable and stable focal mechanism solution. Earthquake source parameters of class A (*i.e.*, a misfit of the waveform fitting <0.3 and a non-double couple component <10%) are used to delineate the depth and surface trace of the MTF, and the geometry of the Longitudinal valley fault (LVF, blue line with triangles) and Luzon arc thrust (green line with triangles) (Fig. 9). Earthquake source parameters of class B (*i.e.*, a misfit of the waveform fitting 0.3–0.5 and non-double couple component <10%) are shown in Fig. S2.

~22 class A pure left-lateral strike-slip events and left-lateral strike-slip events with a thrust component located west of the Longitudinal valley (light red beach balls) are selected in boxes B to F (Fig. 9A). They span from 22.35°N to 23.85°N. Amongst them, 7 are pure left-lateral strike-slip events observed from 22.35°N to 23.45°N, including events marked 1, 2 and 3 (Table 1). They are located along the left-lateral strike-slip Yuli fault (the specific name of the MTF in this area) (red line in Fig. 9A). All these earthquakes focal mechanism 'beach balls' are

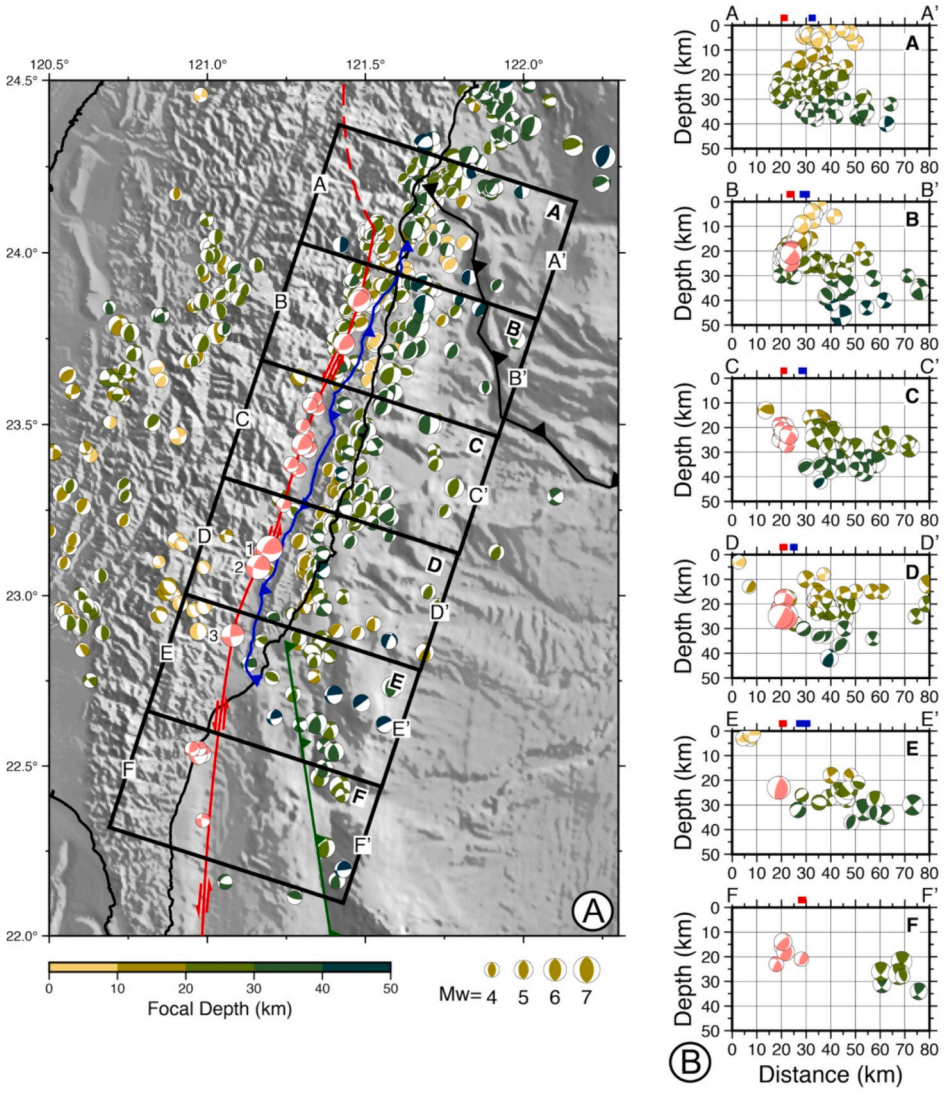

Fig. 9. Focal mechanisms and main geological features in East Taiwan and adjacent offshore area.
The red line is the Manila transcurrent fault (MTF). The blue line with triangles pointing to the east is the Longitudinal valley subduction fault (LVF). The green line with triangles pointing to the east is a shallow <30 km thrust fault with a shear component (Lewis et al., 2015; Chen et al., 2019). A) Distribution of focal mechanisms compiled from the archived AutoBATS moment tensor catalog during the March 1996–December 2023 period (Institute of Earth Sciences, Taiwan, 1996). The deepest seismic events are on top of the shallowest ones. Class A focal mechanisms are plotted in a lower hemisphere projection with different sizes and colours depending on each event's magnitude and hypocentral depth. Light red beach balls are AutoBATS events selected along the Yuli shear fault, which corresponds to the location of the MTF west of the Longitudinal valley. Earthquake source parameters of events 1, 2 and 3 located in boxes D and E appear in Table 1. B) Vertical profiles AA' to CC' located in Fig. 9A show the hypocentral distribution and focal mechanisms inside black boxes in Fig. 9A and plotted in the back-hemisphere projection. Red and blue marks above the X-axis are the location of the MTF and LVF in each black box of Fig. 9A. (For interpretation of the references to colour in this figure legend, the reader is referred to the web version of this article.)

Table 1
Earthquake source parameters from the AutoBATS catalog and location of the Manila transcurrent fault (MTF) called the Yuli left-lateral shear fault located in the Yuli belt, west of the Longitudinal valley basin.

Event No.	Time(year/month/day/h/min/s)	Longitude (°E)	Latitude (°N)	Depth(km)	Mw	Strike (°)	Dip (°)	Rake (°)
1 (Class B)	2022/09/18/06/44/15.25	121.1958	23.1370	25	7.00	210.5	56.3	40.4
2 (Class B)	2022/09/17/13/41/19.11	121.1608	23.0840	25	6.53	201.4	61.5	15.0
3 (Class C)	2006/04/01/10/02/19.54	121.0806	22.8835	23	6.15	177.0	72.4	9.6

at the vertical of Yuli fault marked by the red rectangle on the X-axis, at depths between 15 and 25 km (profiles BB' to FF' in Fig. 9B).

~20 class B events, including 9 pure left-lateral strike-slip events, were found from 22.30°N to 23.90°N, at depths between 15 and 32 km on Fig. S2. Thus, the moment tensor solutions globally show that the vertical left-lateral shear Yuli fault is a crustal feature down to a maximum depth of 32 km from 22.30°N to 23.90°N.

Earthquake focal mechanisms (Fig. 9 and Fig. S2) shows that east of the Longitudinal valley basin, the LVF system (blue line with triangles) and the Luzon arc thrust system (green line with triangles) are oblique thrusts with a left-lateral component of slip. Based on MCS data (Kuo-Chen et al., 2023), the eastward dipping LVF system outcrops east of the Longitudinal valley plain and does not affect the alluvions of the Longitudinal valley. GPS data (Yu and Kuo, 1999) and left-lateral strike-slip faulting suggest that the LVF is a PSP intra-plate deformation feature. The west Luzon arc thrust system, which is in the southern prolongation of the LVF system, with a slightly different orientation, presents the same characteristics. Thus, these two features can be considered as PSP intra-plate deformation with respect to the complex kinematic context of a major vertical shear fault (the MTF) observed further south between the two subduction zones of opposite vergence (Manila trench and East Luzon trough-Philippine trench).

When was the MTF active? Since ~7 Ma, the intra-oceanic Luzon forearc arc and then the Luzon arc, which belong to the PSP, started to collide with the EU continent (Lin et al., 2003; Mesalles et al., 2014; Huang et al., 2018) and glide along the Yuli left-lateral shear fault. ~20 km size blocks of Luzon arc and forearc clockwise rotated 30° (Barrier et al., 1991; Lee et al., 1991), and became parallel to the present-day orientation of the Longitudinal valley. Sedimentary basin sequences formed simultaneously were intermingled within the Coastal range rotated volcanic blocks (Huang et al., 2018). Thus, since ~7 Ma, rotated blocks of the Luzon arc were starting to glide along the MTF at a velocity of ~40 km/Ma, encompassing an orthogonal shortening of ~10 km/Ma (Sibuet et al., 2021). Since ~7 Ma, the intra-plate deformation was observed both in the EU and PSP plates. The westward PSP/EU compressive component was absorbed along the shear thrust faults (also

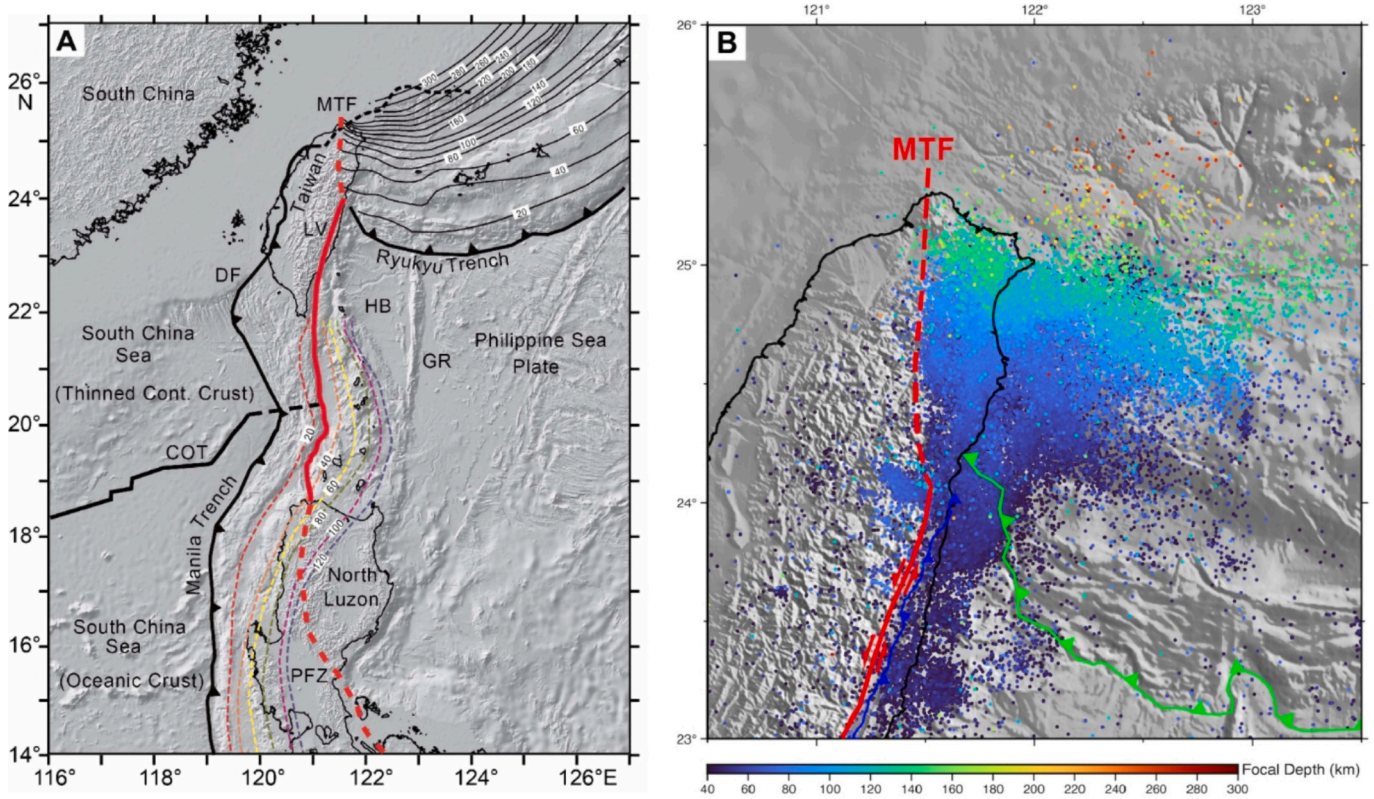

Fig. 10. Relationship between the Manila transcurrent fault (MTF)-Philippine fault zone (PFZ) with respect to Ryukyu and Manila slab geometries.
A) North of 19.3°N, the MTF follows the ~30 km colour contour depth of the Manila slab and then merge the Longitudinal valley (LV). North of the LV, the Ryukyu slab depth isolines abuts against the northern portion of MTF (dashed red line). South of 19.3°N, the MTF and the PFZ (dashed red line) do not show any relationship with the Manila slab depth isolines. B) 1990–2020 earthquakes extracted from the catalog of relocated events using a 3D *Vp* model tomography (Wu et al., 2007, 2008, 2009b) with magnitude ≥3.0 and a hypocenter depth ≥ 40 km. To draw the depth isoline map of Fig. 10A with a 20 km interval, each depth isoline of the Ryukyu slab was determinded by selecting earthquakes in a bandwidth of 2 km on each side of the depth isoline (see north Taiwan earthquakes depth slices in Fig. S4) and by computing the corresponding fitting isoline. The same process was used to determine the Manila slab isolines, for depths comprised between 20 and 120 km. COT, continent-ocean transition zone; DF, Deformation front; GR, Gagua ridge; HB, Huatung basin. (For interpretation of the references to colour in this figure legend, the reader is referred to the web version of this article.)

along the left-lateral shear Yuli fault) in Taiwan and along their offshore prolongations in the EU plate, and in the PSP plate, along the LVF system, the Luzon arc thrust, and the Gagua ridge (Lewis et al., 2015; Liu et al., 2022). Since ~7 Ma, the oblique convergence of the PSP plate (pushed by the Pacific plate) with respect to the EU plate makes an angle of 23° with the NS orientation of the Manila, ELT and Philippine trenches, explaining why numerous intraplate deformations exist in the EU plate as in the PSP plate.

3.4. The MTF north of the Longitudinal valley

1990–2020 earthquakes were extracted from a catalog of relocated events using a 3D *Vp* model tomography (Wu et al., 2007, 2008, 2009b) with magnitude ≥3.0 and a hypocenter depth ≥ 40 km (Fig. 10B). North of 24°N, an abrupt vertical boundary limits the area with deep earthquakes (Fig. 10B). This vertical lithospheric boundary (dashed red line) is in the northern prolongation of the Yuli left-lateral shear fault as already shown by (Ustaszewski et al., 2012) (Fig. S3). It extends beneath the Tatun volcano and disappears a few kilometers north of the Taiwan coastline. The progressive deepening of the Ryukyu slab from depths of 40 km to 250 km is shown by the distribution of earthquakes in six consecutive depth slices (Fig. S4e to j). The depth isoline map of Fig. 10A was established with the procedure described in Fig. 10 legend. The Ryukyu slab depth isolines abut against the northern portion of the MTF. With depth increasing, the PSP Ryukyu slab edge is in contact with the upper continental crust, the lower continental crust, and the upper mantle of the EU plate. Since 20.5 - ~18 Ma until its collision with EU at ~7 Ma, the upper part of Luzon arc in contact with the Ryukyu trench was either subducting below the Ryukyu trench or partly beheaded during its subduction process (Sibuet and Hsu, 2004; Sibuet et al., 2004), contributing to the overall increase in the volume of the continental crust as do the oceanic plateaus for example. Thus, from ~20.5 - ~18 Ma to ~7 Ma, the Luzon arc (beheaded or not) was constantly adjacent to the MTF and its oldest part is now located in the deepest part of the Ryukyu slab, in contact with the MTF. Since ~7 Ma and the onset of Taiwan uplift, the portion of Luzon arc belonging to the Coastal range, moved northwards simultaneously with the PSP, and subducted along the MTF. As the PSP is moving N307° with respect to the stable EU (*e.g.* Yu and Kuo, 1999), at a velocity of 82 mm/yr since ~7 Ma, a compressional deformation might possibly exist along the brittle parts of the adjacent EU plate. For depths <15 km (Fig. S4a and b), numerous earthquakes are observed east of the MTF, in particular under the Tatun volcano, showing that this tiny part of EU upper crust located above the Ryukyu slab is seismogenic and corresponds to the Tatun volcanic activity.

A series of seven NS profiles is presented between 121°E and 124.5°E (Fig. 11B). The width of each stripe is 50 km. From the 1990–2020 seismicity distribution based on Wu et al. (2007, 2008, 2009b) with magnitude ≥3.0, the slab dip for depths larger than >70 km is ~70° and ~ 55° west and east of 123°E, respectively. Fig. 10A shows that the slab depth isolines change trend from approximately EW to N055° at ~123°N, explaining the resulting eastward decrease of slab dip.

The focal mechanism solutions (beach balls) are derived from the autoBATS catalog (1996–2023) (Institute of Earth Sciences, Taiwan, 1996), with only the best focal mechanism solutions (classes A and B). Theoretically, shallow Ryukyu slab earthquakes are expected to exhibit downdip extension due to the negative buoyancy of the plate. Subsequently, as the plate subducts and encounters resistance, downdip-compression earthquakes are anticipated. However, both downdip-extension and downdip-compression earthquakes are observed at different depths (Fig. 11B), without any reliable rule, except that downdip-compression only exists along BB' and GG' profiles. The complexity of the stress field in the Ryukyu slab cannot be explained solely by theory. However, intermediate-depth earthquakes in the northern Ryukyu arc show consistently downdip-extension to a depth of 200 km (Kao et al., 1998; Kao and Chen, 1991). As the resulting PSP/EU present-day motion occurs along the ~NS MTF with compressional deformation of the adjacent PSP and EU plates, it suggests that the downdip-extension observed in northern Ryukyu arc might be polluted by downdip-compression earthquakes in the southern Ryukyu

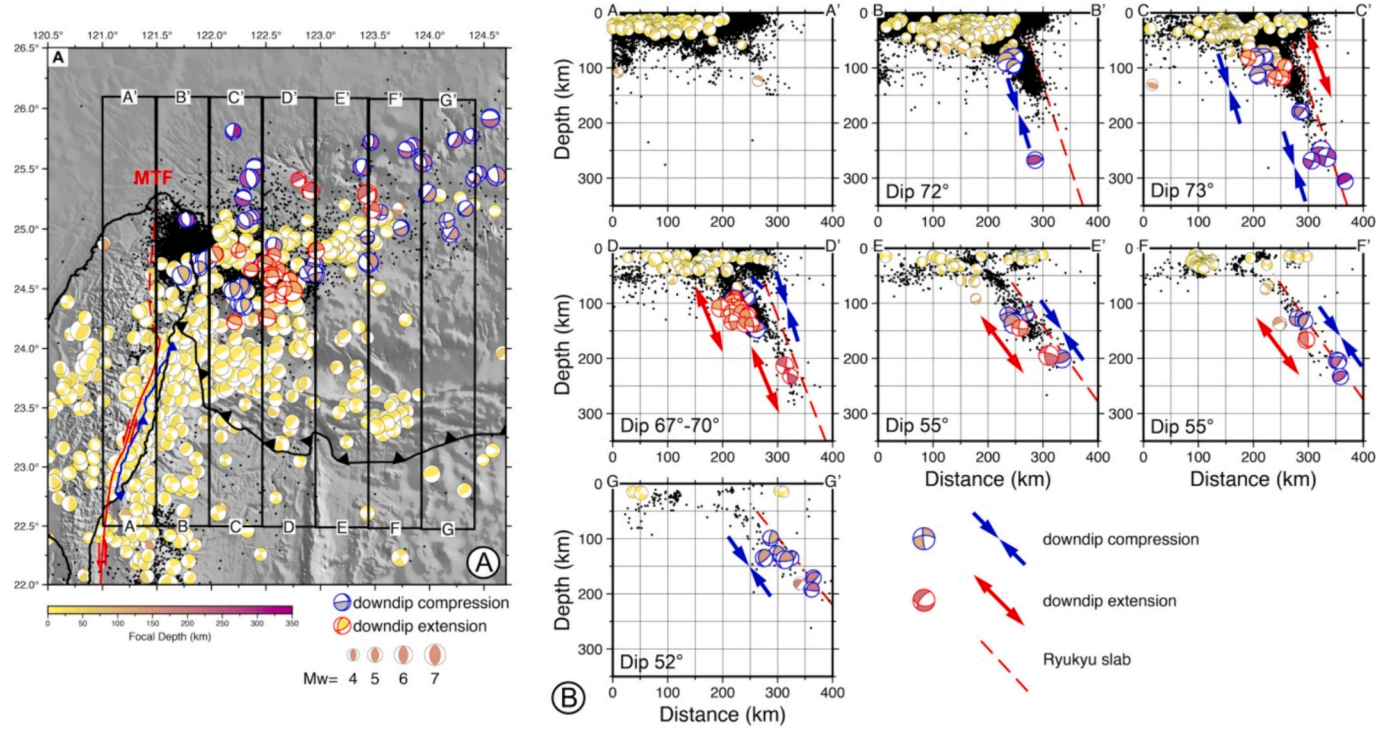

Fig. 11. Focal mechanism solutions show both downdip-extension and -compression in the southern Ryukyu slab.
The focal mechanism solutions (beach balls) are derived from the autoBATS catalog (1996–2023), with only the better focal mechanism solutions (classes A and B). The seismicity distribution (1990–2020) is based on Wu et al. (2007, 2008, 2009b) with magnitude ≥3.0.

subduction zone.

4. Structure of the northeastern South China Sea margin

Exhumed mantle does not exist on the northeastern SCS margin (Larsen et al., 2018; Sun et al., 2019b; Ding et al., 2020; Nirrengarten et al., 2020; Wang et al., 2022; Zhang et al., 2021; Liu et al., 2022) except one possible instance of exhumed mantle that was suggested in the southern part of Profile OBS2016–2 (Wan et al., 2019) but questioned by the presence of oceanic crust along the easternmost portion of MCS Profile MGL0905–17 (McIntosh et al., 2014; Sibuet et al., 2021) (Fig. 5). Other serpentinized bodies defined by gravity modeling below the north Luzon trough forearc basin and below the Coastal range (Doo et al., 2016) do not exist as they are identified within the allochthonous terranes located east of the MTF (Liu et al., 2022). The only place in the northeastern SCS where such an exhumed mantle might exist would be below the post-rift sediments of the failed rift located near the Manila trench at 21.5°N (Fig. 5) (McIntosh et al., 2014; Chen et al., 2023). Thus, the northeastern SCS margin does not seem to belong to the magma-poor margin rubric characterized by exhumed mantle at their COTs. Similarly, the absence of seaward dipping reflectors (SDR) sequences shows that the northeastern SCS margin does not belong to the magma-rich margin rubric. Recently, Pérez-Gussinyé et al. (2023) introduced the rubric "intermediate margins" to characterize the nature of conjugate margins of the SCS, the Woodlark basin, the Gulf of California, or the Red Sea. Below we will discuss the belonging of the SCS to the "intermediate margins" rubric.

The reconstructed northeastern SCS and NW Palawan margins in a pre-breakup position (Nirrengarten et al., 2020), based on Franke et al. (2011) and Larsen et al. (2018) conjugate profiles, shows a wide-rifted zone. The thinned to hyper-thinned basins (*e.g.* Liwan and Bayun basins) on the northeastern SCS margin, separated by basement highs over a width of ~400 km, faces a conjugate ~200 km-wide NW Palawan continental margin fragment (*e.g.* Lai et al., 2021). In fact, the NE Palawan margin belongs to a narrow sliver of continental crust detached from south China and drifted away from the northeastern SCS margin. This ~100 km-wide sliver, which includes part of Palawan and part of Mindoro (Lai et al., 2021; Ding et al., 2023; Fu et al., 2024), rifted away South China as a consequence of continuous proto-SCS subduction (*e.g.* Wu et al., 2016). Thus, the SCS East basin does not belong to the "intermediate margins" rubric of Pérez-Gussinyé et al. (2023) as the Woodlark basin, the Gulf of California, or the Red Sea but to another rubric called the "marginal basins" rubric.

The main characteristic of continental margins of a marginal basin is its complexity. The following information concerns the IODP drilling area, between 116°E and 117°E, where a major effort to understand its structure and geodynamic evolution has been made and will only be briefly recalled in this paragraph. In this area, the COT decreases in width from 28 km in the west to 15 km with an abrupt flip in detachment polarity implying a transfer zone to explain the segmentation of the margin (*e.g.* Larsen et al., 2018; Zhang et al., 2021; Zhao et al., 2023). Such segmentation might result from inherited pre-rift crustal and/or lithospheric weaknesses and is accommodated by the interplay of tectonic and magmatic processes (Zhang et al., 2021). The magma intruded in the COT as dikes and sills, or extruded as volcanoes suggesting magmatic additions, might have been emplaced before, during and/or after rifting (Larsen et al., 2018; Sun et al., 2019b; Nirrengarten et al., 2020; Zhang et al., 2021; Wang et al., 2022). South of the oceanward limit of the COT, fresh pillow basalts and MORBs were collected at IODP drilled sites U1500, U1503 and possibly U1502 (Sun et al., 2019b; Zhang et al., 2021). This oceanward limit of the COT (quoted in Fig. 5 as a 20-km wide zone in light purple) coincides with a main free-air gravity gradient (Taylor, 2017; Liu et al., 2018; Zhang et al., 2021) and is located at the southern boundary of ridge A.

Between 115°E and 118°E, seismic data document a 15 to 25 km wide COT (light purple stripe in Fig. 5), with a similar width than in the IODP Expeditions area (Ding et al., 2020). A short-period magmatic event seems to occur during the latest stage of continental rifting (34–30 Ma), triggering crustal breakup and onset of steady-state seafloor spreading (Ding et al., 2020; Zhang et al., 2021). Variable along-strike *syn*-breakup magmatic activity and a prominent variability in structural style and intensity leads to the specific structure and topography of the COT, suggesting a balancing mechanism between the volume of magmatic additions and faulting styles (Zhang et al., 2021).

Further east, between 119° and 120°E, the NE-SW oriented volcanic ridge D (Fig. 5) is located within the COT. This ridge is in the same structural position with respect to the oceanic domain than the EW oriented ridge A located landside of oceanic crust in the IODP area (Sun et al., 2019b). They might have a common syn and/or post-rift geological history.

Between 120° and 121°E, the COT seems to be ~N80° oriented (black dashed line with light purple stripe in Fig. 5) and to abut against the MTF (Liu et al., 2022). As this portion of COT is partly located below the thick Manila accretionary wedge (Hengchun ridge), its trend is poorly controlled. North of it, the northeastern SCS thinned continental crust is described in section 3.2, with slightly different velocity-depth profiles in the thinned continental crust on each side of the VDB (Figs. 5 and 8).

5. When and how did Okinawa trough open?

As for the end of SCS seafloor spreading, the onset of OT opening was largely debated: 8 Ma (Lallemand et al., 1997, 2001), 10 Ma (Miki, 1995; Shinjo, 1999; Shinjo et al., 1999) or 12 Ma (Sibuet et al., 1995). The timing of the first phase of OT opening (Table 2) was finally established from the volcanic and sedimentary rocks collected on the Ryukyu island volcanic arc. Ishigaki and Yonaguni islands (Figs. 5 and 12) rotated 25° clockwise from ~10 Ma to ~7 Ma (Miki, 1995) while Myako and northern Ryukyu arc islands drifted away without clockwise rotation (as the pole of rotation was ~90° away) during the same period (Miki, 1995; Sibuet et al., 1995; Shinjo, 1999; Shinjo et al., 1999). After a period of quiescence without OT opening between ~7 and ~ 2 Ma (Miki, 1995; Shinjo et al., 1999; Sibuet et al., 1995; Sibuet et al., 2021), a second phase of OT opening began 1–2 Ma ago and is still active today (Miki, 1995; Sibuet et al., 1995; Shinjo et al., 1999; Huang et al., 2018) (Table 2). The propagation of a tear fault in direction of the future northern Taiwan started ~18 Ma ago (Lallemand et al., 1997, 2001; Sibuet et al., 2021), between ~20.5 and ~ 18 Ma in this paper. The boundary between the oceanic and continental domains was defined on the Wu et al. (2016) MITP08 tomography (COB Old in Figs. 5 and 12A). From the onset of the tear between ~20.5 - ~ 18 Ma and ~ 10 Ma, the tear fault follows the location of the COB Old trajectory, simultaneously with the northwestward subduction of the PSP plate and HB in between the two lips of the tear fault. Since the onset of OT opening, ~10 Ma ago, the tear fault trajectory propagated westward and was located south of the Ryukyu forearc.

The present-day COB is located at the rear of the Yaeyama ridge along the COB New feature (Figs. 5 and 12B) (Sibuet et al., 2021). The distance between COB Old and COB New lines is 100 km ±40 km in the east and null at their intersection (Sibuet et al., 2021). Independently, Sibuet et al. (2021) also show that along the NS refraction profile P1 shot

Table 2
Timing of Okinawa trough backarc basin opening.

Before ~20.5–18 Ma	No extension at the location of the future OT backarc basin
~20.5–18 Ma - ~10 Ma	No extension at the location of the future OT backarc basin
~10 Ma - ~7 Ma	First phase of OT backarc basin extension
~7 Ma - ~2 Ma	No extension in the OT backarc basin
~2 Ma - 0 Ma	Second phase of OT backarc basin extension

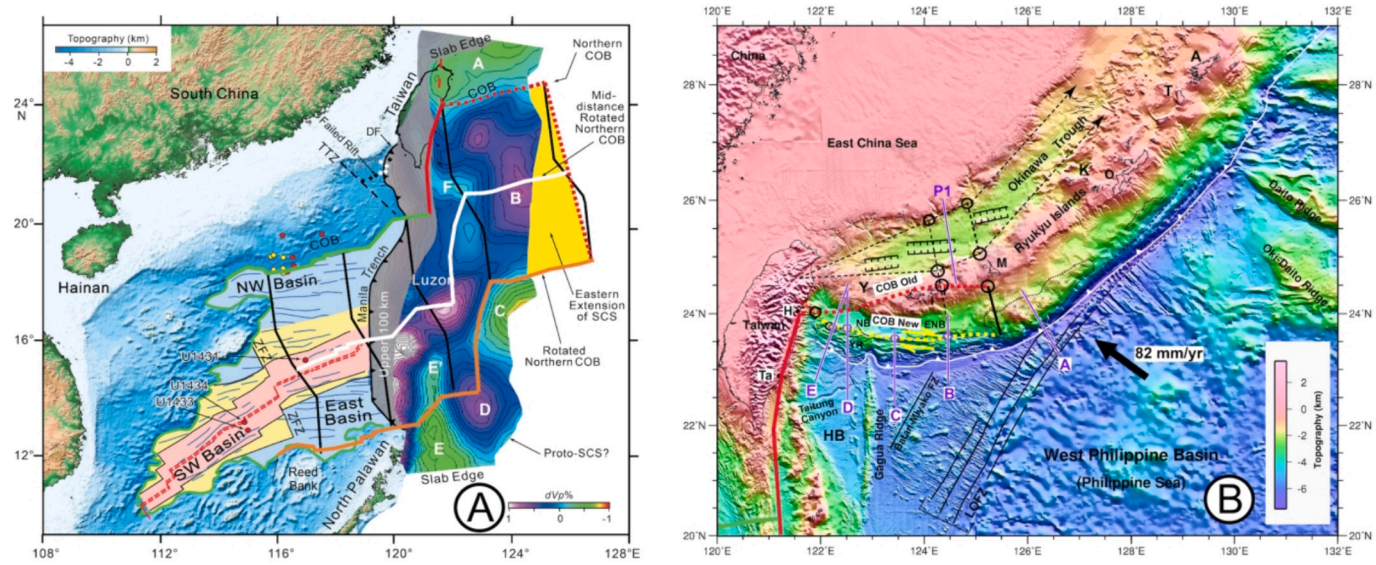

Fig. 12. South China Sea (SCS) oceanic domain with unfolded Manila slab and opening of the Okinawa trough (OT).
A) The unfolded Manila slab is colored by its intra-slab tomographic velocities *dVp* (Wu et al., 2016) and is attached to the SCS along the Manila trench. The NS grey shadow mask (<100 km width) corresponds to probable artifacts and was not interpreted. Seafloor spreading flowlines in black are from Sibuet et al. (2016). The northern COB rotated with respect to Eurasia (EU) (in orange) follows the observed southern COB (green line). The mid-distance rotated northern COB (in white) closely follows the extinct spreading ridge located in the Present SCS. The NNW oriented dashed red line (located east of the yellow area) is the suggested eastern limit of the oceanic SCS domain before becoming the location of the Manila trench initiation (Sibuet et al., 2021). Areas A, B, C, D, E, E' and F are discussed in the text. Yellow and red dots are drilling sites of the International Ocean Drilling Program; DF, Deformation front; TTZ, Taiwan transfer zone; ZFZ, Zhongnan fracture zone. B) Bathymetric map (Hsu et al., 2013) showing the location of the COB before the OT opening (COB Old, red dashed line) and today (COB New, yellow dashed line) (Sibuet et al., 2021). The COB New is located at the rear of the Yaeyama ridge (YR). The area between COB Old and COB New gives the amount of extension during the whole OT opening (Fig. 5) transferred in the OT basin between the black dashed lines. A, Amami island; ENB, east Nanao basin; H, Hualien city; HB, Huatung basin; I, Ishigaki island; K, Kume island; M, Miyako island; NB, Nanao basin; O, Okinawa island; T, Tokuno island; Ta, Taitung city; Y, Yonaguni island. (For interpretation of the references to colour in this figure legend, the reader is referred to the web version of this article.)

across the OT at 124.5°E longitude (Fig. 12B), the OT extension is 100 km ±20 km. Therefore, the two proposed methods, even not very accurate, give an idea of the amount of OT extension west of 125.5°E (southern light green area in Fig. 5). The corresponding whole amount of extension has been transferred in the OT and extended in the northeast with a constant amount of extension as discussed above (northern light green area).

During SCS seafloor spreading (31–32 Ma to ~20.5 - ~18 Ma), the PSP and HB were subducting northwards beneath EU along the Ryukyu trench (Sibuet et al., 2021). We have suggested above that the western boundary of the Ryukyu subduction zone was a left-lateral lithospheric shear zone trending parallel to the HB-PSP/EU plate motion (N307°) along the eastern boundary of the southern light green area (Fig. 5), which was also the eastern limit of the oceanic SCS (dashed red line in Fig. 12A) (Sibuet et al., 2021) called the Manila trench ancestor. The young oceanic SCS started to subduct along this left-lateral shear boundary. However, we are not sure it is a spontaneous subduction initiation as observed in Hjort, Tiburon or Barracuda subduction zones (*e.g.* Arcay et al., 2020).

6. Discussion of kinematic reconstructions

As was previously discussed, the primary factors controlling the kinematic reconstructions are:

a) The onset of the Manila subduction zone occurred during the ~20.5 - ~18 Ma period, a few m.y. before the ~18 Ma oldest age of the intra-oceanic Luzon arc and forearc. The end of the SCS seafloor spreading is already older than 18 Ma and may be as old as ~20.5 Ma (Barckhausen et al., 2014). The Manila trench has always migrated in both time and space. Since ~20.5 - ~18 Ma, the Manila trench shifted ~400-km westward, from 125.5°N to 121.5°N and its orientation changed from N337° to ~north-south today. Since the onset of Luzon arc and forearc collision with EU at ~7 Ma, the intra-plate deformation was observed both in the EU and PSP plates. In the EU plate, the westward PSP/EU compressive component was absorbed along the shear thrust faults in Taiwan and along their offshore prolongations, but also along the left-lateral shear Yuli fault and in the PSP plate, along the LVF system, the Luzon arc system, and the Gagua ridge. The date of the major revolution in the geodynamic evolution of SE Asia is consequently ~7 Ma. Amongst the consequences, the Coastal range abut and remain against the EU continental lithosphere below northern Taiwan. However, it would remain difficult to decipher which thrust fault is an intraplate or a major feature which controls plate motions.

b) Since ~10 Ma, the triangular tip of the OT opening moved with the westward propagation of the tear fault, without OT opening during the phase of OT quiescence from ~7 to ~2 Ma.

Five kinematic reconstructions at critical tectonic periods (Fig. 13) synthesize the main steps of the SE Asia geodynamic evolution since the onset of SCS subduction: 1) from ~20.5 to ~18 Ma: end of SCS seafloor spreading, beginning of westward opening of the tear fault along the COB Old feature; ~20.5 Ma: onset of Manila subduction zone; ~18 Ma: start of Luzon arc and forearc formation. 2) ~10 Ma: start of OT opening. 3) ~7 Ma: forearc and Luzon arc collision, end of first OT opening phase. The MTF started to become active within the portion of thinned continental crust located above the Manila slab. 4) ~2 Ma: beginning of the second OT opening phase.

All plate motions are with respect to Eurasia (South China) (Fig. 13). The plate motions that have occurred since the previous reconstruction are visible on each kinematic reconstruction. Plate boundaries are represented by continuous red lines that indicate the type of motion (shear along the MTF and/or the Manila trench), and extension along the SCS

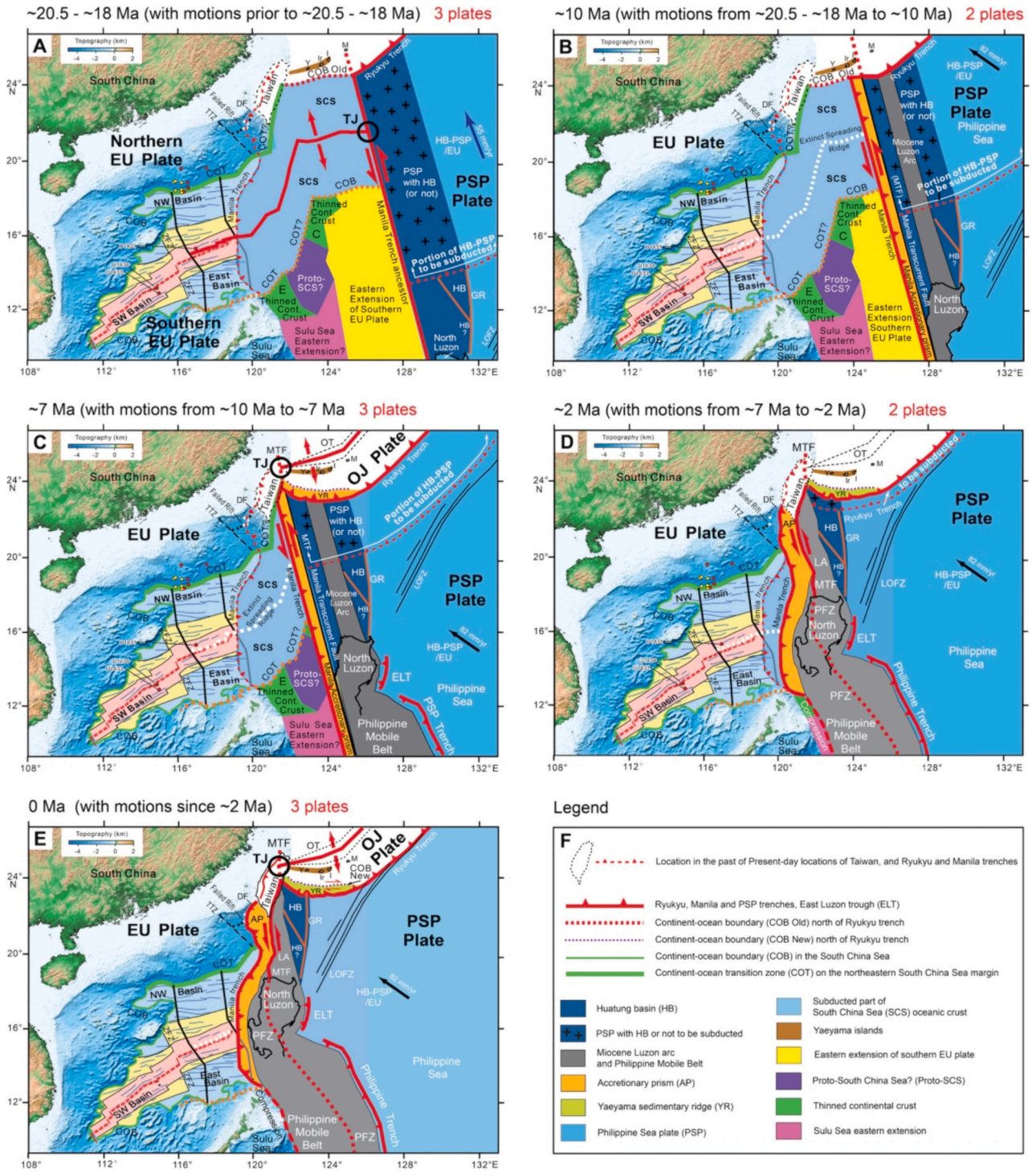

Fig. 13. Kinematic reconstructions at ~20.5 - ~18 Ma, ~10 Ma, ~7 Ma, ~2 Ma and Present (A to E) with motions occurring between a reconstruction and the preceding one.

Continuous red lines are active features from one panel to the preceding one. A major kinematic change occurred ~7 Ma ago when the Luzon forearc and arc collided the EU continent with simultaneous EU and PSP intraplate deformations. F) Legend of main features. AP, Manila accretionary prism; COB, continent-ocean boundary; COT, continent-ocean transition zone; DF, Deformation front; ELT, East Luzon trough; EU, Eurasia; GR, Gagua ridge; HB, Huatung basin; Islands (M, Myako; I, Ishigaki, Ir, Iriomote; Y, Yonaguni); LA, Luzon arc; LOFZ, Luzon-Okinawa fracture zone; MTF, Manila transcurrent fault; OJ, Okinawa-Japan; OT, Okinawa trough; PFZ, Philippine fault zone; PSP, Philippine Sea plate; TJ, Triple junction; TTZ, Taiwan transfer zone; YR, Yaeyama ridge; ZFZ, Zhongnan fracture zone. (For interpretation of the references to colour in this figure legend, the reader is referred to the web version of this article.)

spreading axis and OT ridge axes); the northern part of the MTF is represented by a dashed red line when its surface expression became hidden below the EU crust of northern Taiwan. Active trenches are shown by continuous red lines with triangles. Multiple plate systems are identified (Fig. 14). For each three-plate systems, a RFF (ridge-fault-fault) triple junction is involved, R being the SCS ridge axis before ~20.5 - ~18 Ma or the OT axis between ~10 and ~ 7 Ma, and since ~2 Ma, and F being the MTF or the Manila trench with its left-lateral shear

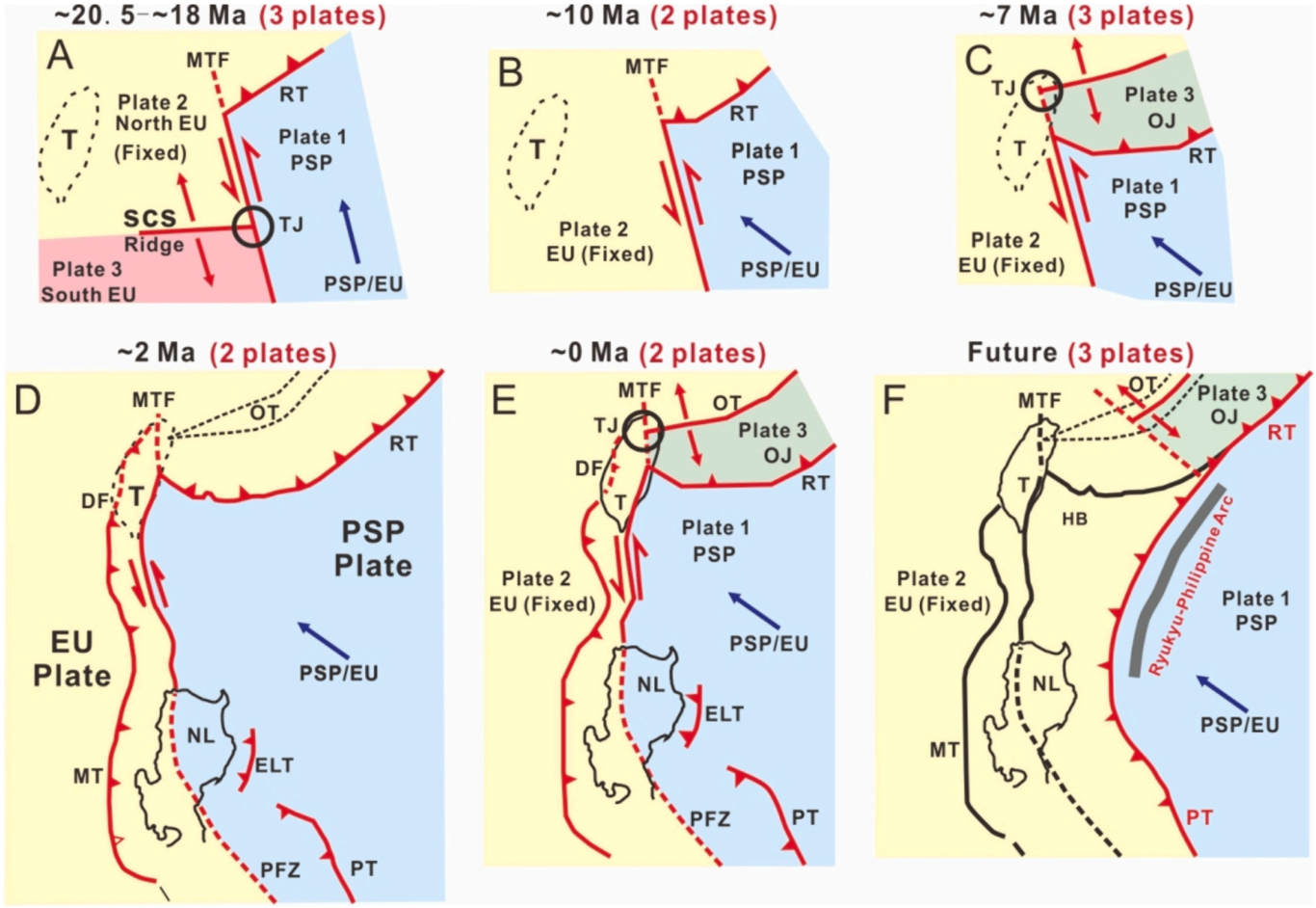

Fig. 14. Kinematic sketches (A to F) with motions occurring between a sketch and the preceding one from ~20.5 - ~18 Ma to future.
The six sketches are all at the same scale. Continuous red lines are active features. DF, Deformation front; ELT, East Luzon trough; EU, Eurasia; HB, Huatung basin; MTF, Manila transcurrent fault; NL, North Luzon island; OJ, Okinawa-Japan; OT, Okinawa trough; PFZ, Philippine fault zone; PSP, Philippine Sea plate; PT, Philippine trench; RT, Ryukyu trench; TJ, Triple junction. (For interpretation of the references to colour in this figure legend, the reader is referred to the web version of this article.)

component (Fig. 13A, C and E). For two-plate systems, the Ryukyu trench and the Manila trench, with its left-lateral shear component, demarcate the boundary between the EU and PSP plates (Fig. 13B and D).

6.1. ~20.5 - ~18 Ma: End of SCS opening and onset of a tear fault

Fig. 13A shows the maximum extent of the SCS oceanic domain at the end of seafloor spreading, ~20.5 - ~18 Ma ago. With respect to the SCS oceanic domain, the northern and southern COT are in green and red, and green and orange respectively. The subducted SCS oceanic domain (light blue) is slightly larger than the present-day SCS domain. To the north, the COB Old (dashed red line) is located between the western limit of the Ryukyu subduction zone and the future location of Taiwan.

Before ~20.5 - ~18 Ma, during SCS seafloor spreading, the SCS spreading center was active (red continuous line in Fig. 13A). The PSP with or without a portion of HB (dark blue with crosses) was subducting below the Ryukyu trench in the N337° direction. The left-lateral shear fault (Manila trench ancestor), which was fixed with respect to EU before ~20.5 - ~18 Ma, was bounding the western end of the Ryukyu subduction zone (Fig. 13A). The absence of tectonic constraints has led to the arbitrary drawing of the Manila trench ancestor as a straight line >1000 km long, which is a likely oversimplification based on arcuate and complex present-day trench geometries. Thus, before ~20.5 - ~18 Ma, a triple junction existed at the contact between the SCS spreading ridge and the Manila trench ancestor. Three plates separated by active plate boundaries (continuous red lines) are identified: the PSP to the east, the northern EU plate to the north and the southern EU plate to the south (Fig. 13A). The southern EU plate includes the southern part of the SCS oceanic basin, the domain located south of the light orange COT, the thinned continental crusts of Palawan, and domains E and C further east (Fig. 13A). Before ~20.5 - ~18 Ma, the SCS spreading ridge axis was moving southward with respect to EU, in the N157° direction (direction opposite to N337°) as shown by the SCS opening trajectories (Figs. 12A, 13A and 14) (Sibuet et al., 2021).

6.2. ~10 Ma: SCS subduction and Luzon arc formation

About ~20.5–18 Ma ago, the first revolution (*i.e.* regional plate organization) took place. The three-plates system active before ~20.5 - ~18 Ma evolved into a two-plates system active since ~20.5 - ~18 Ma and separated by the Manila trench which started to develop along the trend of the former Manila trench ancestor. The PSP, including the possible HB prolongation of the present-day northern HB (dark blue domain with crosses called PSP with HB or not in Fig. 13B), is now subducting in the N307° direction, below the Ryukyu trench. The emergence of Luzon arc and forearc outcrop on the sea-bottom started ~18 Ma ago. The EU plate (reunion of the former northern and southern EU plates) is now the area located outside the Manila trench-Ryukyu

trench system. Between ~20.5 - ~18 Ma and ~ 10 Ma, the active Ryukyu trench extremity was moving westward along the COB Old tear fault, with the PSP progressing northwestward between the two lips of the tear (Figs. 13B and 14). The northward prolongation of the Manila trench (dashed red line) moved in longitude from the Myako to Ishigaki islands, and the Manila accretionary prism grew ahead the Manila trench. However, the sedimentation in the accretionary prism was probably weak, as the sediments from EU were caught by the Ryukyu trench bathymetric depression and the sediments deposited on the recently formed SCS oceanic crust were relatively thin. Thus, the first revolution started between ~18 Ma and ~ 20.5 Ma with the change in the PSP/EU plate motion from N337° to N307° and a change from a three- to two-plate system.

6.3. ~7 Ma: Onset of first phase of Okinawa trough opening and collision of Luzon arc with Eurasia

The second revolution, linked to a significant tectonic and structural shift, happened ~7 Ma ago at the time the first phase of OT opening was coming to a finish and the Luzon forearc and arc collided with the EU near the site of the future Taiwan (Fig. 13C).

From ~10 Ma to ~7 Ma, the tear continued to open and to propagate westward until reaching the EU continent or close to it; the western boundary of the Ryukyu subduction zone was moving simultaneously with the tip of the tear (Fig. 13C). The first phase of OT opening also occurred from ~10 Ma to ~7 Ma while the PSP (with HB or not) continued to subduct below the Ryukyu trench in the N307° direction. During this period, the Ryukyu accretionary prism (Yaeyama ridge) continued to form and to propagate in the westward direction; the Okinawa-Japan plate defined by Sibuet et al. (2004a, b) between the Ryukyu trench and the OT axis was growing in the NS direction, simultaneously with the southward displacement of the Ryukyu forearc and trench with respect to the EU plate. The East Luzon trough and the Philippine trench started to form ~8 Ma ago from north to south (Ozawa et al., 2004) (Figs. 1, 5 and 13C). Note the simultaneous local decrease of convergence between the islands of Palawan and Mindoro with respect to the Luzon island volcanic arc (*e.g.* Lai et al., 2021).

Therefore, from ~10 Ma to ~7 Ma, three plates separated by active plate boundaries (continuous red lines) were identified (Figs. 13C and 14): the PSP to the east, the EU plate, and the Okinawa-Japan plate. The RFF triple junction was located at the intersection of the Manila trench (with its left-lateral strike-slip component) with the OT axis, and progressively moved westward simultaneously with the Manila trench, from the longitude of Ishigaki island to close to Taiwan.

6.4. ~2 Ma: Onset of second phase of Okinawa trough opening

~2 Ma ago, the second phase of Okinawa trough opening started (Table 2). The EU plate continued to subduct below the PSP and only a small portion of non-subducted EU plate (SCS oceanic domain) remained west of the Manila accretionary prism.

Since ~7 Ma, the MTF continued to be active from north of Taiwan (dashed red line), along the Longitudinal valley and further south along the eastern boundary of the Manila accretionary prism (continuous red line), and then along the Philippine fault zone (dashed red line in the Philippine Mobile belt) (Figs. 13D and 14). The grey area in Fig. 13D represents the extent of the Philippine Mobile belt. Since ~7 Ma, the PFZ probably changed trend several times and the Luzon arc and forearc collided with the EU margin. Taiwan terranes uplifted and shortening along Taiwan thrust faults parallel to the Longitudinal valley continued.

6.5. Present-time: Ongoing second phase of Okinawa trough opening and MTF still active

Since ~2 Ma, the second phase of OT opening occurred and is still active today; the Okinawa-Japan plate was growing in the NS direction, simultaneously with the southward displacement of the Ryukyu forearc and trench. As during the first phase of OT opening, we identify a three-plate system with the PSP to the east, the EU plate to the west and the Okinawa-Japan plate. The triple junction is in northern Taiwan, at the point where the OT axis and the MTF converge. North of north Luzon island, the MTF becomes roughly NS oriented (Figs. 13E and 5). Thus, since ~7 Ma, the MTF rotated ~23° clockwise, which roughly corresponds to the estimation of Wu et al. (2016).

6.6. Future SE Asia plate kinematic evolution

Since ~20.5 - ~18 Ma, the MTF has been continuously active and moving westward with respect to the stable EU (South China). However, since ~7 Ma, the amplitude of this motion has decreased near Taiwan, and this has been compensated by a ~ 23° clockwise rotation of the MTF around a pole of rotation that is approximately located north of Taiwan. Therefore, the portion of MTF located north of the Longitudinal valley (dashed red line) only moved a few tens of kilometers westward. Since ~2 Ma, with respect to the stable EU, the OT tip was only propagating a few tens of kilometers westward inside Taiwan. Furthermore, the RFF triple junction is unstable (McKenzie and Morgan, 1969), suggesting that the further evolution of the SE Asia kinematic frame is possible.

Geodynamic numerical modeling shows that face-to-face double subduction systems, as evidenced in SE Asia by the old Ryukyu subduction zone and the ~8 Ma young East Luzon trough-Philippine trench (Ozawa et al., 2004), are dynamically unstable (Zhang et al., 2024). The waxing younger subduction (East Luzon trough and Philippine subduction zone) may gradually absorb the PSP/EU plate convergence previously entirely absorbed by the Ryukyu subduction zone. In such a scenario, the East Luzon and Philippine trenches may join the Ryukyu trench through the Luzon-Okinawa fracture zone (Fig. 15) to favor a new stable system (Zhang et al., 2024). The consequence would be a major simplification of the SE Asia geodynamic framework with the presence of a curved subduction zone and a potential associated backarc basin, except along the Luzon-Okinawa fracture zone where an intra-oceanic volcanic arc and forearc might appear as did the Luzon arc and forearc since ~18 Ma. The Ryukyu subduction zone would be bounded by a feature parallel to the PSP/EU motion and like the MTF segment formed before ~20.5 Ma (dashed red line). Both the present-day Manila subduction zone and MTF (including the Philippine fault zone) would become inactive but the complexity of most existing features, such as the present-day SCS and the Philippine mobile belt, would be preserved (Fig. 15).

7. Conclusions

The main conclusions of this study are as follows:

1) Within a compressive framework dominated by the continually active Sunda subduction zone, the SCS is one of the oceanic basins classified as “marginal basins.” Our ability to identify active plate boundaries and subducted East Asian plates allows us to propose new SE Asia plate kinematic reconstructions.
2) Within the East basin, the end of SCS seafloor spreading varies from 15.5 Ma (Briais et al., 1993) to 20.5 Ma (Barckhausen et al., 2014). Drilling at IODP hole U1431, near the East basin extinct spreading center, revealed sediments and undeformed oceanic crust with Ar^{39}/Ar^{40} ages marginally older than 18 Ma. These ages refute the 15.5–16 Ma estimate of Briais et al. (1993) for the end of SCS seafloor spreading, which might be older than 18 Ma, somewhere in the ~20.5 - ~18 Ma range.
3) The oldest ages of the Luzon arc and forearc obtained in the Lanyu island, Coastal range and Lichi mélange are 17–18 Ma. This indicates that the onset of the Manila subduction zone occurred a few m.y. earlier, perhaps ~20.5 Ma ago, which would account for the age of the first known Luzon arc intrusions.

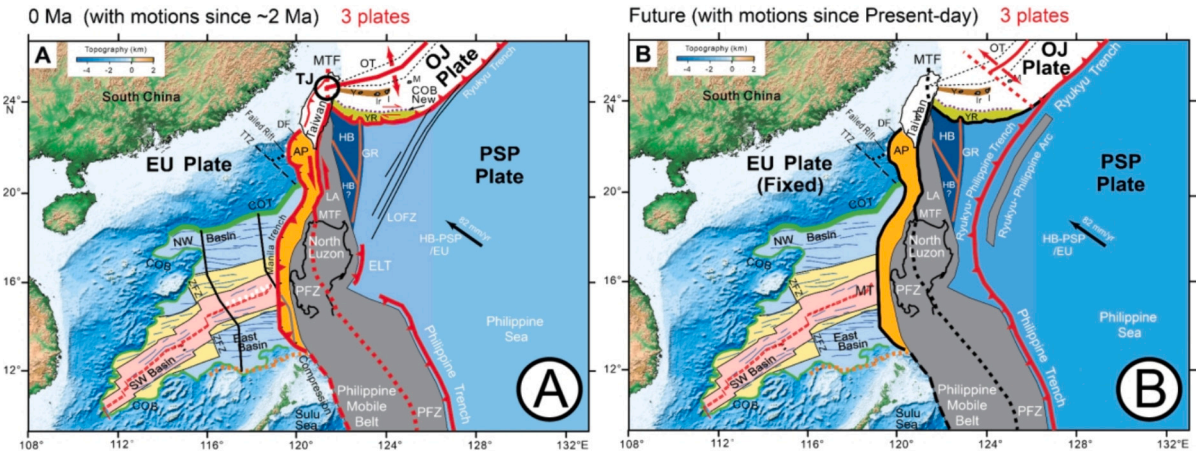

Fig. 15. Present-day (A) and future (B) kinematic reconstructions with motions occurring between a reconstruction and the preceding one. Continuous red lines are active features. Legend of figures as in Fig. 13F. The proposed future kinematic reconstruction is based on numerical modeling, which shows that the process of waxing and waning of subduction zones controls the plate motion reorganization (Zhang et al., 2024). Note the previous major kinematic change occurred at ~7 Ma, when the Luzon forearc and arc collided the EU continent with simultaneous EU and PSP intraplate deformations. AP, Manila accretionary prism; COB, continent-ocean boundary; COT, continent-ocean transition zone; DF, Deformation front; ELT, East Luzon trough; EU, Eurasia; GR, Gagua ridge; HB, Huatung basin; Islands (M, Myako; I, Ishigaki, Ir, Iriomote; Y, Yonaguni); LA, Luzon arc; LOFZ, Luzon-Okinawa fracture zone; MTF, Manila transcurrent fault; NL, North Luzon island; OJ, Okinawa-Japan; OT, Okinawa trough; PFZ, Philippine fault zone; PSP, Philippine Sea plate; PT, Philippine trench; RT Ryukyu trench; TJ, Triple junction; TTZ, Taiwan transfer zone; YR, Yaeyama ridge; ZFZ, Zhongnan fracture zone. (For interpretation of the references to colour in this figure legend, the reader is referred to the web version of this article.)

4) Given that the timing of the SCS opening's end is uncertain, ranging from 20.5 to 18 Ma, it is possible that the SCS seafloor spreading took place during the Manila subduction zone's active phase. Before ~20.5 - ~18 Ma, during the SCS seafloor spreading, the MTF (dashed red line) was a left-lateral shear fault lithospheric segment, which started from the western extremity of the Ryukyu trench to the north. From then until today, that portion of the MTF extending northward from the western end of the Ryukyu trench has always remained active, with the PSP plate subducting in parallel to the PSP/EU vector. From ~20.5 - ~18 Ma to ~7 Ma, the portion of permanent MTF located north of the Ryukyu trench was connected to Manila trench. Since ~7 Ma, the permanent MTF was connected to the longitudinal valley and became a left-lateral crustal shear fault only active above the Manila slab. Further south, the MTF was connected to the Philippine fault zone. Therefore, since before ~20.5 Ma, the MTF moved 400 km westward with respect to EU and since ~7 Ma, rotated ~23° clockwise to become now ~NS oriented north of 16°N.
5) A tear fault was identified in the EU plate north of the Ryukyu trench and south of Myako to Yonaguni islands and was progressively tearing westwards until Taiwan. It was active from ~20.5 - ~18 Ma to ~10 Ma with the PSP subducting northwestward between the two lips of the tear. Since ~10 Ma, the tear continued to progress westward but during each of the two OT opening phases, from ~10 to ~7 Ma and since ~2 Ma, a triple junction was active at the intersection of the OT tip with the MTF. In other words, the tearing point was always on the MTF, which was on the western boundary of the Ryukyu subduction zone. Thus, when active, the triple junction was located on the MTF, with one branch on each side of the triple junction, the third branch being the SCS spreading center before ~20.5–18 Ma and the OT axis from ~10 to ~7 Ma and since ~2 Ma.
6) In the future, the OT tip and the portion of MTF north of the longitudinal valley would not travel forever westward due to the instability of the RFF triple junction. The younger East Luzon trough-Philippine subduction zone might join the present-day Ryukyu subduction zone possibly along the Luzon-Okinawa fracture zone. With this new stable system, both the Manila subduction zone and the MTF (including the PFZ) would become inactive, but most of the present-day SCS features and the Philippine mobile belt would be kept.

CRediT authorship contribution statement

Jean-Claude Sibuet: Writing – review & editing, Writing – original draft, Validation, Supervision, Methodology, Conceptualization. **Siqing Liu:** Writing – review & editing, Visualization, Methodology, Investigation, Funding acquisition, Formal analysis, Data curation. **Minghui Zhao:** Writing – review & editing, Resources, Funding acquisition. **Wen-Nan Wu:** Visualization, Methodology, Investigation, Formal analysis. **Yih-Min Wu:** Methodology, Investigation, Formal analysis. **Jinhui Cheng:** Writing – review & editing, Visualization, Software, Methodology, Formal analysis. **Jonny Wu:** Resources, Conceptualization.

Declaration of competing interest

The authors declare that they have no known competing financial interests or personal relationships that could have appeared to influence the work reported in this paper.

Data availability

The authors do not have permission to share data.

Acknowledgements

This multi-faceted scientific contribution has been developed since July 26, 2022, the date of the disappearance of my wife Myriam Sibuet, deep-sea ecologist. Her kindness, empathy and constant intellectual support allowed me to overcome this difficult period by escaping with her in this scientific quest. Scientific discussions with Chi-Yue Huang, Hongfang Gao, Mengming Yu and Serge Lallemand are deeply acknowledged. We thank Xiaofan Zang who reviewed the manuscript before submission and carefully polished the English language. The GMT software (Wessel and Smith, 1995) was used in this study. This work was supported by the National Natural Science Foundation of China (contract 42106078), the Major Research Plan on West-Pacific Earth System Multi-spheric Interactions (contract 91958212), the Guangzhou Science and Technology Planning Project (contract 2023A04J0243),the Special Fund of South China Sea Institute of Oceanology of the Chinese Academy of Sciences (contract SCSIO2023HC08), and the U.S. National

Science Foundation (contract 1848327). We are also grateful to the crew of the R/V Shiyan 6 as well as scientists and technicians for their precious involvement during the NORC2015-08 and NORC2016-08 cruises.

Appendix A. Supplementary data

Supplementary data to this article can be found online at https://doi.org/10.1016/j.tecto.2024.230397.

References

Advokaat, E.L., Marshall, N.T., Li, S., Spakman, W., Krijgsman, W., van Hinsbergen, D.J. J., 2018. Cenozoic rotation history of Borneo and Sundaland, SE Asia revealed by paleomagnetism, seismic tomography, and kinematic reconstruction. Tectonics 37, 2486–2512. https://doi.org/10.1029/2018TC005010.

Arcay, D., Lallemand, S., Abecassis, S., Garel, F., 2020. Can subduction initiation at a transform fault be spontaneous? Solid Earth Discuss. 11, 37–62. https://doi.org/10.5194/se- 11-37-2020.

Armada, L.T., Hsu, S.-K., Ku, C.-Y., Wu, W.-N., Dimalanta, C., Yumul Jr., G., 2013. Possible northward extension of the Philippine Fault zone offshore Luzon Island (Philippines). Mar. Geophys. Res. 33, 369–377. https://doi.org/10.1007/s11001-013-9169-5.

Aurelio, M.A., 2000. Shear partitioning in the Philippines: Constraints from Philippine Fault and global positioning system data. Island Arc 9, 584–597.

Aurelio, M.A., Barrier, E., Gaulon, R., Rangin, C., 1997. Deformation stress states along the central segment of the Philippine Fault: implications to wrench fault tectonics. J. Asian Earth Sci. 15, 107–119.

Aurelio, M., Forbes, M.T., Taguibao, K.J.L., Savella, R.B., Bacud, J.A., Franke, D., Pubellier, M., Savva, D., Meresse, F., Steuer, S., Carranza, C.D., 2014. Middle to late Cenozoic tectonic events in south and Central Palawan (Philippines) and their implications to the evolution of the south-eastern margin of South China Sea: evidence from onshore structural and offshore seismic data. Mar. Pet. Geol. 58, 658–673. https://doi.org/10.1016/j.marpetgeo.2013.12.002.

Barckhausen, U., Engels, M., Franke, D., Ladage, S., Pubellier, M., 2014. Evolution of the South China Sea: revised ages for breakup and seafloor spreading. Mar. Pet. Geol. 58, 599–611. https://doi.org/10.1016/j.marpetgeo.2014.02.022.

Barrier, E., Huchon, P., Aurelio, M., 1991. Philippine fault: a key for Philippine kinematics. Geology 19, 32–35. https://doi.org/10.1130/0091-7613(1991)019<0032:PFAKFP>2.3.CO;2.

Boutonnet, E., Arnaud, N., Guivel, C., Lagabrielle, Y., Scalabrino, B., Espinoza, F., 2010. Subduction of the South Chile active spreading ridge: a 17 Ma to 3 Ma magmatic record in Central Patagonia (western edge of Meseta del Lago Buenos Aires, Argentina). J. Volcanol. Geotherm. Res. 189 (3–4), 319–339. https://doi.org/10.1016/j.jvolgeores.2009.11.022.

Briais, A., Patriat, P., Tapponnier, P., 1993. Updated interpretation of magnetic anomalies and seafloor spreading stages in the South China Sea: Implications for the Tertiary tectonics of Southeast Asia. J. Geophys. Res. 98, 6299–6328.

Chen, W.-H., Huang, C.-Y., Yan, Y., Dilek, Y., Chen, D., Wang, M.-H., Zhang, X., Lan, Q., Yu, M., 2017. Stratigraphy and provenance of forearc sequences in the Lichi Mélange, Coastal Range: Geological records of the active Taiwan arc-continent collision. J. Geophys. Res. 122, 7408–7436. https://doi.org/10.1002/2017JB014378.

Chen, W.S., Wu, Y.M., Yeh, P.Y., Lai, Y.X., Ke, M.C., Ke, S.S., Lin, Y.K., 2019. Seismogenic Structures of the Subduction-collision Transitional Zone in Southeastern Taiwan Offshore, 34. Special Publication, Center Geological Survey, MOEA, pp. 125–140 (in Chinese with English abstract).

Chen, C., Yan, P., Yu, J., Zhong, G., 2023. Seismically imaged crustal breakup in the Southwest Taiwan Basin of the northeastern South China Sea margin. Geochem. Geophys. Geosyst. 24 https://doi.org/10.1029/2023GC010918 e2023GC010918.

Chi, W.-R., Suppe, J., 1985. Tectonic implications of Miocene sediments of Lan-Hsü Island, northern Luzon arc. Pet. Geol. Taiwan 21, 93–106.

Conand, C., Mouthereau, F., Ganne, J., Lin, A.T., Lahfid, A., Daudet, M., Mesalles, L., Giletycz, S., Bonzani, M., 2020. Strain partitioning and exhumation in oblique Taiwan collision: Role of rift architecture and plate kinematics. Tectonics 38. https://doi.org/10.1029/2019TC005798.

Deng, H., Ren, J., Pang, X., Rey, P.F., McClay, K.R., Watkinson, I.M., Zheng, J., Luo, P., 2020. South China Sea documents the transition from wide continental rift to continental break up. Nat. Commun. 11, 4583. https://doi.org/10.1038/s41467-020-18448-y.

Ding, W., Sun, Z., Mohn, G., Nirrengarten, M., Tugend, J., Manatschal, G., Li, J., 2020. Lateral evolution of the rift-to-drift transition in the South China Sea: evidence from multi-channel seismic data and IODP Expeditions 367&368 drilling results. Earth Planet. Sci. Lett. 531, 115932 https://doi.org/10.1016/j.epsl.2019.115932.

Ding, W., Zhu, R., Wan, B., Zhao, L., Niu, X., Zhao, P., Sun, B., Zhao, Y., 2023. Geodynamic processes of the southeastern Neo-Tethys Ocean and the formation mechanism of the curved subduction system in Southeast Asia. Sci. China Earth Sci. 66 (4), 703–717. https://doi.org/10.1007/s11430-022-1071-4.

Doo, W.-B., Kuo-Chen, H., Brown, D., Lo, C.-L., Hsu, S.-K., Huang, Y.-S., 2016. Serpentinization of the fore-arc mantle along the Taiwan arc-continent collision of the northern Manila subduction zone inferred from gravity modeling. Tectonophysics 69, 282–289. https://doi.org/10.1016/j.tecto.2016.10.019.

Eakin, D.H., McIntosh, K.D., Van Avendonk, H.J.A., Lavier, L., Lester, R., Liu, C.-S., Lee, C.-S., 2014. Crustal-scale seismic profiles across the Manila subduction zone: the transition from intraoceanic subduction to incipient collision. J. Geophys. Res. 119, 1–17. https://doi.org/10.1002/2013JB010395.

Eakin, D.H., McIntosh, K.D., Van Avendonk, H.J.A., Lavier, L., 2015. New geophysical constraints on a failed subduction initiation: the structure and potential evolution of the Gagua Ridge and Huatung Basin. Geochem. Geophys. Geosyst. 16, 380–400. https://doi.org/10.1002/2014GC005548.

Franke, D., Barckhausen, U., Baristeas, N., Engels, M., Ladage, S., Lutz, R., Montano, J., Pellejera, N., Ramos, E.G., Schnabel, M., 2011. The continent-ocean transition at the southeastern margin of the South China Sea. Mar. Pet. Geol. 28 (6), 1187–1204. https://doi.org/10.1016/j.marpetgeo.2011.01.004.

Fu, X., Gao, S., Zhu, W., 2024. The Northeast Mindoro block is the conjugate margin of the southern East China Sea Basin: Insight from detrital zircon data. Mar. Pet. Geol. https://doi.org/10.1016/j.marpetgeo.2024.106710.

Guan, Q.S., Zhang, T., Taylor, B., Gao, J.Y., Li, J.B., 2021. Ridge jump reorientation of the South China Sea revealed by high-resolution magnetic data. Terra Nova. https://doi.org/10.1111/ter.12532.

Hsu, S.-K., Yeh, Y.-C., Sibuet, J.-C., Doo, W.-B., Tsai, C.-H., 2013. A mega-splay fault system and tsunami hazard in the southern Ryukyu subduction zone. Earth Planet. Sci. Lett. 362, 99–107. https://doi.org/10.1016/j.epsl.2012.11.053.

Huang, C.Y., Xia, K., Yuan, P.B., Chen, P.G., 2001. Structural evolution from Paleogene extension to latest Miocene-recent arc-continent collision offshore Taiwan: comparison with on land geology. J. Asian Earth Sci. 19 (5), 619–638. https://doi.org/10.1016/S1367-9120(00)00065-1.

Huang, C.-Y., Chen, W.-H., Wang, M.-H., Lin, C.-T., Yang, S., Li, X., Yu, M., Zhao, X., Yang, K.-M., Liu, C.-S., Hsieh, Y.-H., Harrish, R., 2018. Juxtaposed sequence stratigraphy, temporal-spatial variations of sedimentation and development of modern-forming forearc Lichi Mélange in North Luzon Trough forearc basin onshore and offshore eastern Taiwan: an overview. Earth Sci. Rev. 182, 102–140. https://doi.org/10.1016/j.earscirev.2018.01.015.

Institute of Earth Sciences, Taiwan, 1996. Broadband Array in Taiwan for Seismology. Institute of Earth Sciences, Academia Sinica Taiwan. https://doi.org/10.7914/SN/TW.

Jian, P.R., Tseng, T.L., Liang, W.T., Huang, P.H., 2018. A new automatic full-waveform regional moment tensor inversion algorithm and its applications in the Taiwan Area. Bull. Seismol. Soc. Am. 108 (2), 573–587. https://doi.org/10.1785/0120170231.

Kao, H., Chen, W.P., 1991. Earthquakes along the Ryukyu-Kyushu arc: Strain segmentation, lateral compression, and the thermomechanical state of the plate interface. J. Geophys. Res. 96 (21), 443–485.

Kao, H., Shen, S.-S.J., Ma, K.-F., 1998. Transition from oblique subduction to collision: Earthquakes in the southernmost Ryukyu arc-Taiwan region. J. Geophys. Res. 103, 7211–7229 (doi:10.29/97jb03510).

Karig, D.E., 1971. Origin and development of marginal basins in the western Pacific. J. Geophys. Res. 76 (11), 2542–2561.

Koppers, A.P., 2014. On the $^{40}Ar/^{39}Ar$ Dating of Low-Potassium Ocean Crust Basalt from IODP Expedition 349, South China Sea: 2014 AGU Fall Meeting, T31E-03.

Kuo-Chen, H., Brown, D., Lai, S.-Y., Chen, J.-Y., 2023. Reflection seismic profiling along the Longitudinal Valley Basin, Eastern Taiwan: in search of the Central Range fault. Tectonophysics 869, 230129. https://doi.org/10.1016/j.tecto.2023.230129.

Lai, C.-K., Xia, X.-P., Hall, R., Meffre, S., Tsikouras, B., Balangue-Tarriela, M.I.R., Idrus, A., Ifandi, E., Norazme, N., 2021. Cenozoic evolution of the Sulu Sea arc-basin system: an overview. Tectonics 40. https://doi.org/10.1029/2020TC006630 e2020TC006630.

Lallemand, S., 2016. Philippine Sea plate inception, evolution and consumption: focus on the newly named Deschamps seamount fringing the Central Basin Fault Rift in memory of Anne Deschamps. Prog. Earth Planet. Sci. 3 (15), 1–26. https://doi.org/10.1186/s40645-016-0085-6.

Lallemand, S.E., Liu, C.-S., Font, Y., 1997. A tear fault boundary between the Taiwan orogen and the Ryukyu subduction zone. Tectonophysics 274, 171–190.

Lallemand, S., Font, Y., Bijwaard, H., Kao, H., 2001. New insights on 3-D plates interaction near Taiwan from tomography and tectonic implications. Tectonophysics 335, 229–253. https://doi.org/10.1016/S0040-1951(01)00071-3.

Lallemand, S., Theunissen, T., Schnürle, P., Lee, C.-S., Liu, C.-S., Font, Y., 2013. Indentation of the Philippine Sea plate by the Eurasia plate in Taiwan: details from recent marine seismological experiments. Tectonophysics 594, 60–79. https://doi.org/10.1016/j.tecto.2013.03.020.

Larsen, H.C., Mohn, G., Nirrengarten, M., Sun, Z., Stock, J., Jian, Z., Klaus, A., Alvarez-Zarikian, C.A., Boaga, J., Bowden, S.A., Briais, A., Chen, Y., Cukur, D., Dadd, K., Ding, W., Dorais, M., Ferré, E.C., Ferreira, F., Furusawa, A., Gewecke, A., Hinojosa, J., Höfig, T.W., Hsiung, K.H., Huang, B., Huang, E., Huang, X.L., Jiang, S., Jin, H., Johnson, B.G., Kurzawski, R.M., Lei, C., Li, B., Li, L., Li, Y., Lin, J., Liu, C., Liu, C., Liu, Z., Luna, A.J., Lupi, C., McCarthy, A., Ningthoujam, L., Osono, N., Peate, D.W., Persaud, P., Qiu, N., Robinson, C., Satolli, S., Sauermilch, I., Schindlbeck, J.C., Skinner, S., Straub, S., Su, X., Su, C., Tian, L., van der Zwan, F.M., Wan, S., Wu, H., Xiang, R., Yadav, R., Yi, L., Yu, P.S., Zhang, C., Zhang, J., Zhang, Y., Zhao, N., Zhong, G., Zhong, L., 2018. Rapid transition from continental breakup to igneous oceanic crust in the South China Sea. Nat. Geosci. 11, 782–789. https://doi.org/10.1038/s41561-018-0198-1.

Lee, T.-Q., Kissel, C., Barrier, E., Laj, C., Chi, W.-R., 1991. Paleomagnetic evidence for a diachronic clockwise rotation of the Coastal Range, eastern Taiwan. Earth Planet. Sci. Lett. 104 (2–4), 245–257.

Lee, J.-C., Angelier, J., Chu, H.-T., 1997. Polyphase history and kinematics of a complex major fault zone in the northern Taiwan mountain belt: the Lishan fault. Tectonophysics 274, 97–115.

Lewis, J.C., O'Hara, D.J., Rau, R.-J., 2015. Seismogenic strain across the transition from fore-arc slivering to collision in southern Taiwan. J. Geophys. Res. 120 https://doi.org/10.1002/2015JB011906.
Li, C., Xu, X., Lin, J., Sun, Z., Zhu, J., Yao, Y., Zhao, X., Liu, Q., Kulhanek, D.K., Wang, J., 2014. Ages and magnetic structures of the South China Sea constrained by deep tow magnetic surveys and IODP Expedition 349. Geochem. Geophys. Geosyst. 15, 4958–4983. https://doi.org/10.1002/2014GC005567.
Li, C.F., Lin, J., Kulhanek, D.K., the Expedition 349 Scientists, 2015a. Expedition 349 summary. In: Proceedings of the International Ocean Discovery Program, 349. https://doi.org/10.14379/IODP.PROC.349.101.2015.
Li, C.F., Lin, J., Kulhanek, D.K., Williams, T., Bao, R., Briais, A., Brown, E.A., Chen, Y., Clift, P.D., Colwell, F.S., Dadd, K.A., Ding, W., Hernández-Almeida, I., Huang, X.-L., Hyun, S., Jiang, T., Koppers, A.A.P., Li, Q., Liu, C., Liu, Q., Liu, Z., Nagai, R.H., Peleo-Alampay, A., Su, X., Sun, Z., Tejada, M.L.G., Trinh, H.S., Yeh, Y.-C., Zhang, C., Zhang, F., Zhang, G.-L., Zhao, X., 2015b. Site U1431. In: Li, C.F., Lin, J., Kulhanek, D. K., the Expedition 349 Scientists (Eds.), *Proceedings of the International Ocean Discovery Program, 349: South China Sea Tectonics:* College Station, TX (International Ocean Discovery Program). https://doi.org/10.14379/iodp.proc.349.103.2015.
Lin, A.T., Watts, A.B., Hesselbow, S.P., 2003. Cenozoic stratigraphy and subsidence history of the South China Sea margin in the Taiwan region. Basin Res. 15, 453–478. https://doi.org/10.1046/j.1365-2117.2003.00215.x.
Liu, S.Q., Zhao, M.H., Sibuet, J.-C., Qiu, X.L., Wu, J., Zhang, J.Z., Chen, C.X., Xu, Y., Sun, L.T., 2018. Geophysical constraints on the lithospheric structure in the northeastern South China Sea and its implications for the South China Sea geodynamics. Tectonophysics 742–743, 101–119. https://doi.org/10.1016/j.tecto.2018.06.002.
Liu, S., Gao, J., Zhao, M., Sibuet, J.-C., 2022. Crustal structure of the northern Manila subduction zone: is thinned continental crust or oceanic crust subducting beneath the Luzon arc and forearc? Tectonophysics 844, 229605. https://doi.org/10.1016/j.tecto.2022.229605.
Lo, Y.C., Chen, C.T., Lo, C.H., Chung, S.L., 2020. Ages of ophiolitic rocks along plate suture in Taiwan orogen: fate of the South China Sea from subduction to collision. Terr. Atmos. Ocean. Sci. 31, 383–402.
McIntosh, K., Lavier, L., Van Avendonk, H.J.A., Lester, R., Eakin, D., 2014. Crustal structure and inferred rifting processes in the northeast South China Sea. Mar. Pet. Geol. 58, 612–626. https://doi.org/10.1016/j.marpetgeo.2014.03.012.
McKenzie, D.P., Morgan, W.J., 1969. Evolution of triple junctions. Nature 224 (5215), 125–133.
Mesalles, L., Mouthereau, F., Bernet, M., Chang, C.-P., Lin, A.T., Fillon, C., Sengelen, X., 2014. From submarine continental accretion to arc-continent orogenic evolution: the thermal record in southern Taiwan. Geology 42, 907–910. https://doi.org/10.1130/G35854.1.
Mi, L., Deng, H., Gouiza, M., Yang, H., Sun, Q., Sun, S., Dong, F., 2023. Crust necking of the northeastern South China Sea: Insights from deep seismic data. Ital. J. Geosci. 142 https://doi.org/10.3301/IJG.2023.06.
Miki, M., 1995. Two-phase opening model for the Okinawa Trough inferred from paleomagnetic study of the Ryukyu arc. J. Geophys. Res. 100, 8169–8184.
Mohn, G., Ringenbach, J.-C., Nirrengarten, M., Lei, C., McCarthy, A., Tugend, J., 2022. Mode of continental breakup of marginal seas. Geology 50 (10), 1208–1213.
Nayak, K., Lin, A.T.-S., Huang, K.-F., Liu, Z., Babonneau, N., Ratzov, G., Pillutla, R.K., Das, P., Hsu, S.-K., 2021. Clay-mineral distribution in recent deep-sea sediments around Taiwan: Implications for sediment dispersal processes. Tectonophysics 814, 228974. https://doi.org/10.1016/j.tecto.2021.228974.
Nirrengarten, M., Mohn, G., Kusznir, N.J., Sapin, F., Despinois, F., Pubellier, M., Chang, S.P., Larsen, H.C., Ringenbach, J.C., 2020. Extension modes and breakup processes of the Southeast China-Northwest Palawan conjugate rifted margins. Mar. Pet. Geol. 113 https://doi.org/10.1016/j.marpetgeo.2019.104123.
Ozawa, A., Tagami, T., Listanco, E.L., Arpa, C.B., Sudo, M., 2004. Initiation and propagation of subduction along the Philippine Trench: evidence from the temporal and spatial distribution of volcanoes. J. Asian Earth Sci. 23, 105–111. https://doi.org/10.1016/S1367-9120(03)00112-3.
Pérez-Gussinyé, M., Collier, J.S., Armitage, J.J., Hopper, J.R., Sun, Z., Ranero, C.R., 2023. Towards a process-based understanding of rifted continental margins. Nat. Rev. Earth Environ. 4, 166–184. https://doi.org/10.1038/s43017-022-00380-y.
Polvé, M., Maury, R.C., Jégo, S., Bellon, H., Margoum, A., Yumul Jr., G.P., Payot, B.D., Tamayo Jr, R.A.T., Cotten, J., 2007. Temporal geochemical evolution of neogene magmatism in the Baguio Gold–Copper Mining District (Northern Luzon, Philippines). Resour. Geol. 57, 197–218. https://doi.org/10.1111/j.1751-3928.2007.00017.x.
Qian, S., Salters, V., McCoy-West, A.J., Wu, J., Rose-Koga, E.F., Nichols, A.R.L., Zhang, L., Zhou, H., 2022. Highly heterogeneous mantle caused by recycling of oceanic lithosphere from the mantle transition zone. Earth Planet. Sci. Lett. 593, 117679 https://doi.org/10.1016/j.epsl.2022.117679.
Shinjo, R., 1999. Geochemistry of high Mg andesites and the tectonic evolution of the Okinawa Trough - Ryukyu arc system. Chem. Geol. 157, 69–88.
Shinjo, R., Chung, S.-L., Kato, Y., Kimura, M., 1999. Geochemical and Sr-Nd isotopic characteristics of volcanic rocks from the Okinawa Trough and Ryukyu arc: Implications for the evolution of a young, intra-continental back arc basin. J. Geophys. Res. 104 (10), 591–608.
Sibuet, J.-C., Hsu, S.-K., 2004. How was Taiwan created? Tectonophysics 379, 159–181. https://doi.org/10.1016/j.tecto.2003.10.022.
Sibuet, J.-C., Hsu, S.-K., Shyu, C.-T., Liu, C.-S., 1995. Structural and kinematic evolution of the Okinawa Trough Backarc Basin. In: Taylor, B. (Ed.), Backarc Basins: Tectonics and Magmatism. Plenum Press, New York, pp. 343–378.
Sibuet, J.-C., Hsu, S.-K., Debayle, E., 2004. In: Clift, P., Wang, P., Kuhnt, W., Hayes, D.E. (Eds.), Geodynamic Context of the Taiwan Orogen. Continent-Ocean interactions within East Asian Marginal Seas, 149. American Geophysical Union Monograph, Washington, D.C., pp. 127–158
Sibuet, J.-C., Yeh, Y.-C., Lee, C.-S., 2016. Geodynamics of the South China Sea. Tectonophysics 692, 98–119. https://doi.org/10.1016/j.tecto.2016.02.022.
Sibuet, J.-C., Zhao, M.H., Wu, J., Lee, C.-S., 2021. Geodynamic and plate kinematic context of South China Sea subduction during Okinawa trough opening and Taiwan orogeny. Tectonophysics 817, 1–19. https://doi.org/10.1016/j.tecto.2021.229050.
Sisson, V.B., Pavlis, T.L., Roeske, S.M., Thorkelson, D.J., 2003. Introduction: an overview of ridge-trench interactions in modern and ancient settings. Geology of a transpressional orogen developed during ridge-trench interaction along the North Pacific margin. In: Sisson, V.B., Roeske, S.M., Pavlis, T.L. (Eds.), Geological Society of America Special Paper, Boulder, Colorado, vol. 371, pp. 1–18.
Sun, Z., Ding, W.W., Zhao, X.X., Qiu, N., Lin, J., Li, C.F., 2019a. The latest spreading periods of the South China Sea: New constraints from macrostructure analysis of IODP Expedition 349 cores and geophysical data. J. Geophys. Res. 124 (10), 9980–9998. https://doi.org/10.1029/2019JB017584.
Sun, Z., Lin, J., Qiu, N., Jian, Z.M., Wang, P.X., Pang, X., Zheng, J.Y., Zhu, B.D., 2019b. The role of magmatism in the thinning and breakup of the South China Sea continental margin. Natl. Sci. Rev. 6 (5), 871–876. https://doi.org/10.1093/nsr/nwz116.
Taylor, B., 2017. The rifting to spreading evolution of marginal basins. In: 2017 AGU Fall Meeting Abstract, T32A-02, New Orleans, LA.
Ustaszewski, K., Wu, Y.-M., Suppe, J., Huang, H.-H., Chang, C.-H., Carena, S., 2012. Crust–mantle boundaries in the Taiwan-Luzon arc-continent collision system determined from local earthquake tomography and 1D models: Implications for the mode of subduction polarity reversal. Tectonophysics 578, 31–49. https://doi.org/10.1016/j.tecto.2011.12.029.
van de Lagemaat, S.H.A., van Hinsbergen, D.J.J., 2024. Plate tectonic cross-roads: reconstructing the Panthalassa-Neotethys junction region from Philippine Sea Plate and Australasian oceans and orogens. Gondwana Res. 126, 129–201. https://doi.org/10.1016/j.gr.2023.09.013.
Wan, X.L., Li, C.F., Zhao, M.H., He, E.Y., Liu, S.Q., Qiu, X.L., Lu, Y., Chen, N., 2019. Seismic velocity structure of the magnetic quiet zone and continent-ocean boundary in the northeastern South China Sea. J. Geophys. Res. 124 (11), 866–899. https://doi.org/10.1029/2019JB017785.
Wang, Q., Zhao, M.H., Zhang, J.Z., Zhang, H.Y., Sibuet, J.-C., Li, Z.Z., He, E.Y., Qiu, X.L., Peng, W., Chen, G.Z., 2022. Breakup mechanism of the northern South China Sea: evidence from the deep crustal structure across the continent-ocean transition. Gondwana Res. 120, 47–69. https://doi.org/10.1016/j.gr.2022.09.004.
Wessel, P., Smith, W.H.F., 1995. New version of the generic mapping tools released. Eos. Trans. 76, 329.
Wu, J., Suppe, J., 2018. Proto-South China Sea plate tectonics using subducted slab constraints from tomography. J. Earth Sci. 29 (6), 1304–1318. https://doi.org/10.1007/s12583-017-0813-x.
Wu, J.T., Wu, J., 2019. Izanagi-Pacific ridge subduction revealed by a 56 to 46 Ma magmatic gap along the northeast Asian margin. Geology 47 (10), 953–957. https://doi.org/10.1130/G46778.1.
Wu, Y.-M., Chang, C.-H., Zhao, L., Shyu, J.B.H., Chen, Y.-G., Sieh, K., Avouac, J.-P., 2007. Seismic tomography of Taiwan: improved constraints from a dense network of strong motion stations. J. Geophys. Res. 112, B08312. https://doi.org/10.1029/2007JB004983.
Wu, Y.-M., Chang, C.-H., Zhao, L., Teng, L.T., Nakamura, M., 2008. A comprehensive relocation of earthquakes in Taiwan from 1991 to 2005. Bull. Seismol. Soc. Am. 98, 1471–1481. https://doi.org/10.1785/0120070166.
Wu, Y.-M., Shyu, J.B.H., Chang, C.-H., Zhao, L., Nakamura, M., Hsu, S.-K., 2009b. Improved seismic tomography offshore northeastern Taiwan: implications for subduction and collision processes between Taiwan and the southernmost Ryukyu. Geophys. J. Int. 178, 1042–1054. https://doi.org/10.1111/j.1365-246X.2009.04180.x.
Wu, J., Suppe, J., Lu, R., Kanda, R., 2016. Philippine Sea and East Asian plate tectonics since 52 Ma constrained by new subducted slab reconstruction methods. J. Geophys. Res. 121, 4670–4741. https://doi.org/10.1002/2016JB012923.
Wu, Z., Zhang, J., Xu, M., Li, H., 2023. Magnetic anomaly lineations in the Northeastern South China Sea and their implications for initial seafloor or spreading. Front. Earth Sci. 10, 1015856. https://doi.org/10.3389/feart.2022.1015856.
Yu, S.B., Kuo, L.C., 1999. GPS observation of crustal deformation in the Taiwan-Luzon region. Geophys. Res. Lett. 26, 923–926.
Yu, S.-B., Kuo, L.-C., 2001. Present-day crustal motion along the Longitudinal Valley Fault, eastern Taiwan. Tectonophysics 333, 199–217. https://doi.org/10.1016/S0040-1951(00)00275-4.
Zhang, C., Sun, Z., Manatschal, G., Pang, X., Li, S., Sauter, D., Péron-Pinvidic, G., Zhao, M.H., 2021. Ocean-continent transition architecture and breakup mechanism at the mid-northern South China Sea. Earth Sci. Rev. 217, 103620 https://doi.org/10.1016/j.earscirev.2021.103620.
Yu, M.M., Yumul, G.P., Dilek, Y., Yan, Y., Huang, C.-Y, 2022. Diking of various slab melts beneath forearc spreading center and age constraints of the subducted slab. Earth and Planetary Science Letters 579, 117367. https://doi.org/10.1016/j.epsl.2022.117367.
Zhang, K., Liao, J., Gerya, T., 2024. Onset of double subduction controls plate motion reorganization. Nat. Commun. 15, 1513. https://doi.org/10.1038/s41467-024-44764-8.
Zhao, M.H., Sibuet, J.-C. Wu, Jonny., 2019. Intermingled fates of the South China Sea and Philippine Sea plate. Natl. Sci. Rev. 6 (5), 886–890. https://doi.org/10.1093/nsr/nwz107.
Zhao, Z., Sun, Z., Qiu, N., Zhao, M., Zhang, J., Li, F., Lin, J., Lee, E.Y., 2023. The paleo-lithospheric structure and rifting-magmatic processes of the northern South China

Sea passive margin. Gondwana Res. 120, 162–174. https://doi.org/10.1016/j.gr.2022.06.015.